Multiparticle interference in electronic Mach-Zehnder interferometers

D. L. Kovrizhin[1,2] and J. T. Chalker[1]

[1]*Theoretical Physics, Oxford University, 1 Keble Road, Oxford OX1 3NP, United Kingdom*
[2]*RRC Kurchatov Institute, 1 Kurchatov Square, Moscow 123182, Russia*
(Received 5 January 2010; revised manuscript received 29 March 2010; published 22 April 2010)

We study theoretically electronic Mach-Zehnder interferometers built from integer quantum-Hall-edge states, showing that the results of recent experiments can be understood in terms of multiparticle interference effects. These experiments probe the visibility of Aharonov-Bohm (AB) oscillations in differential conductance as an interferometer is driven out of equilibrium by an applied bias, finding a lobe pattern in visibility as a function of voltage. We calculate the dependence on voltage of the visibility and the phase of AB oscillations at zero temperature, taking into account long-range interactions between electrons in the same edge for interferometers operating at a filling fraction $\nu=1$. We obtain an exact solution via bosonization for models in which electrons interact only when they are inside the interferometer. This solution is nonperturbative in the tunneling probabilities at quantum-point contacts. The results match observations in considerable detail provided the transparency of the incoming contact is close to one-half: the variation in visibility with bias voltage consists of a series of lobes of decreasing amplitude and the phase of the AB fringes is practically constant inside the lobes but jumps by π at the minima of the visibility. We discuss in addition the consequences of approximations made in other recent treatments of this problem. We also formulate perturbation theory in the interaction strength and use this to study the importance of interactions that are not internal to the interferometer.

I. INTRODUCTION

Recent experiments[1–10] on electronic Mach-Zehnder interferometers (MZIs) constructed from integer quantum-Hall-edge states have attracted a great deal of attention. In these experiments Aharonov-Bohm (AB) oscillations are observed in the differential conductance of the interferometer. The most striking results concern behavior at finite bias voltage. The visibility of AB oscillations shows a series of lobes as a function of voltage while their phase is independent of bias, except near visibility minima where it changes sharply by π. Our concern in this paper is with the theoretical understanding of these experiments.

The observations are interesting from several perspectives. First, as was quickly appreciated,[2] it is plausible that the effects arise from electron-electron interactions, because behavior of this kind does not occur in a single-particle model. In addition, more seems to be required than a simple treatment in which inelastic scattering leads only to decoherence since approaches of that kind cannot produce multiple side lobes in visibility of AB oscillations with increasing bias. It is remarkable that electron interactions should have the distinctive signatures found in this system since integer quantum-Hall-edge states are usually modeled in the low-energy limit as a chiral Fermi gas of independent particles.[11] The experiments therefore appear to reflect interaction physics that is not captured by the standard, universal description, but is robust enough to appear in many devices of varying designs. A second reason for interest stems from current efforts[12–20] to study interferometry in fractional quantum-Hall states as a probe of fractional or non-Abelian quasiparticle statistics. Against that background it is clearly important to understand unexpected interaction effects in much simpler, integer quantum-Hall systems. A third reason for interest is

that the phenomenon seems to be an example of coherent many-body physics in a quantum system far from equilibrium. It invites comparison with other nonequilibrium quantum problems, from the Kondo effect[21] to cold atomic gases.[22]

The design of an experimental device working as an MZI is shown in Fig. 1. It uses the edge states of a two-dimensional electron gas that is in an integer quantum-Hall plateau. (Most experiments have been done at filling factor $\nu=2$ but broadly similar results have also been reported at $\nu=1$). The edge states serve as electron waveguides and are coupled at quantum point contacts (QPCs), which act as beam splitters. Current between, for example, source S1 and drain D2 is measured as a function of the voltage difference applied between sources S1 and S2. Interference fringes are observed as oscillations in the differential conductance either when the magnetic-flux density is varied by a small amount or when a side gate is used to change the interferometer area or arm lengths. The visibility and phase of these oscillations vary with voltage in the fashion already summarized. A physical scale is set by the bias voltage at which the first minimum in visibility occurs: the measured value, about 14 μV in the first experiment,[2] corresponds roughly to the chemical potential increase required to add one electron to an edge state with length equal to that of the interferometer arms: for arm length d and edge velocity v_F, this chemical potential increase is $\hbar v_F/d$.

Theoretical studies of coherence in electronic MZIs started before these experiments. Early work treated dephasing arising from a variety of possible sources: interactions within the interferometer;[23] a fluctuating classical field;[24,25] voltage probes;[26] or coupling to an external quantum bath.[27] None of these approaches generates the subsequently observed lobe pattern in the dependence of visibility on bias voltage. A further calculation,[28] based on a microscopic treat-
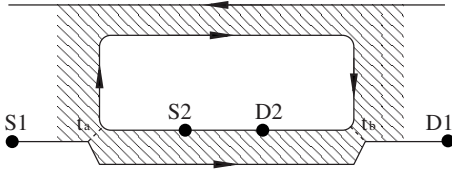
FIG. 1. Schematic view of the electronic Mach-Zehnder interferometer, which consists of a Hall bar with an island in it. A two-dimensional electron gas in a quantum-Hall plateau occupies the shaded region. One edge state propagates along the lower edge of the Hall bar, from source S1 to drain D1, and a second edge state propagates around the island, from source S2 to drain D2. Tunneling between these two edge states takes place at two quantum point contacts, with amplitudes t_a and t_b, at the points indicated by dashed lines.

ment of the effects of long-range interactions and using bosonization combined with a perturbative treatment of tunneling at the QPCs, shows that nonmonotonic variations in visibility can appear for weakly coupled edge states, but without capturing the features found experimentally. By contrast, studies of models with additional structure, involving either a counterpropagating edge mode[29] or the pair of edge modes that arise at filling factor $\nu=2$,[30] show that resonances can appear in that setting, which lead to lobes in visibility similar to those observed. These results are encouraging but (as we discuss in Sec. VIII) the models involved seem to us insufficiently generic to account for all experiments. More recently, approximate treatments of the effects of interactions at $\nu=1$ when edges are strongly coupled by QPCs have generated some of the behavior found experimentally.[31–33] There is good reason to think that these calculations identify some of the relevant physics but the approximations used are nonstandard and their domain of validity is unclear.

In this paper we set out a detailed treatment of interaction effects in MZIs at filling factor $\nu=1$. The approach is microscopic in the sense that it is based on the standard Hamiltonian for quantum-Hall-edge states[11] and does not involve external noise. Our main results come from the exact solution of models which have one simplifying feature: interactions that are restricted to the interior of the MZI; a short account of this part of our work has been presented previously.[34] We also present work in three further directions. One of these is an elementary solution of the two-particle problem, which is a simplification of ideas from Ref. 33. We believe that this calculation provides a useful illustration of the essential physics behind the phenomena we are concerned with, which is multiparticle interference. A second direction is a careful analysis of the approximations involved in Ref. 32. The third direction is the formulation of perturbation theory in interaction strength, which allows us to assess the importance of interactions that extend beyond the interior of the MZI.

The organization of rest of the paper is as follows. The two-particle problem is addressed in Sec. II and the general microscopic description of the MZI is set out in Sec. III. In Sec. IV we show how models with interactions only in the interior of the interferometer can be solved exactly. In Sec. V we use this approach to study interferometers with various
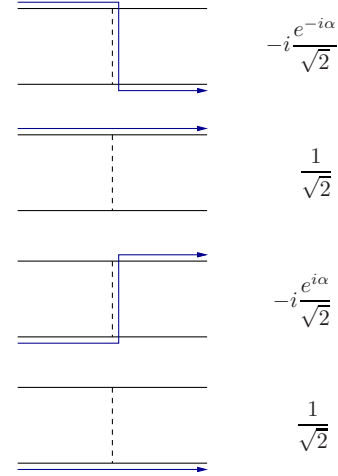

FIG. 2. (Color online) Possible paths and associated scattering amplitudes at a single QPC with transmission probability 1/2. The phase α of the transmission amplitude is unimportant for a single QPC but contributes to the AB phase in an MZI.

interaction potentials. We present an extended discussion of Ref. 32 in Sec. VI and develop perturbation theory in interaction strength in Sec. VII. We summarize our conclusions in Sec. VIII. Some technical details of the calculations are given in appendices.

II. TWO-PARTICLE PROBLEM

In this section we set out a pedagogical treatment of the two-particle problem that illustrates how electron interactions affect the visibility of AB oscillations in an MZI. We consider an interferometer having both arms of the same length d and a propagation velocity v_F for electrons. Denoting their separation by s, the flight time during which both are inside the interferometer is $\tau=(d-s)/v_F$. We take the two electrons to interact with a potential energy U when both are inside the MZI on the same edge but not to interact otherwise. For simplicity, we consider first the case in which the magnitudes of the transmission amplitudes at the two QPCs are $t_a=t_b=1/\sqrt{2}$, giving results for the general case later.

We solve the scattering problem for an initial state in which both particles are positioned on the upper channel before the first contact. We evaluate the probability for one or both particles to exit the interferometer in the lower channel by summing all quantum-mechanical amplitudes that connect the initial state to a given final state. We regard the expectation value for the total charge transferred from the upper channel to the lower channel as the analog for the two-particle problem of the current in the many-body, steady-state case.

To establish some notation, consider in the first instance single-particle scattering, initially for one QPC and then for an MZI. Amplitudes for the four scattering processes at one QPC are shown in Fig. 2, and the two possible paths through an MZI between an initial state in the upper channel and a final state in the lower channel are shown in Fig. 3. The amplitudes associated with these two paths are given by products of the amplitudes arising at each QPC. Taking the
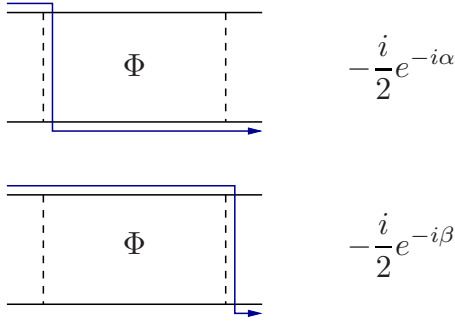
FIG. 3. (Color online) Possible paths and associated amplitudes for a single particle to propagate through an MZI from an initial state on the upper channel to a final state on the lower channel. The phase difference $\Phi = \beta - \alpha$ is the AB phase arising from enclosed flux. The combined amplitude A for transitions between these states is the sum of contributions from the two paths: $A = -ie^{-i(\alpha+\beta)/2} \cos(\Phi/2)$. The total current is proportional to $|A|^2 = \frac{1}{2}[1 + \cos\Phi]$.

total current to be proportional to the transition probability between the upper and lower channels, one obtains the standard result given in the caption to Fig. 3, with oscillations in the current as a function of the AB phase Φ.

Now consider the two-particle problem with an initial state as described, in which both particles are on the upper channel. Paths to a final state with both particles in the lower channel are shown in Fig. 4 and those to a final state with one particle in each channel in Fig. 5. (Because there is no dispersion, particles cannot exchange positions in the scattering process. They may therefore be treated as if they were distinguishable and this is reflected in the figures by the use of different colors for the paths of each particle.) Without interactions the amplitude for a given pair of paths would
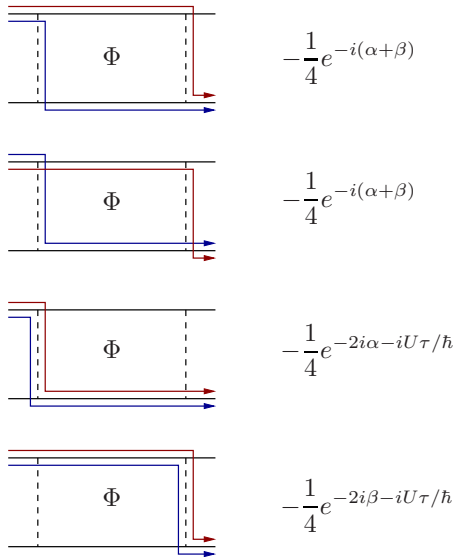

FIG. 4. (Color online) The four possible paths and associated amplitudes for two particles to propagate through an MZI from an initial state with both particles on the upper channel to a final state with both particles on the lower channel. The combined amplitude is $A_2 = -\frac{1}{2}e^{-i(\alpha+\beta)}[1 + e^{iU\tau/\hbar}\cos\Phi]$.
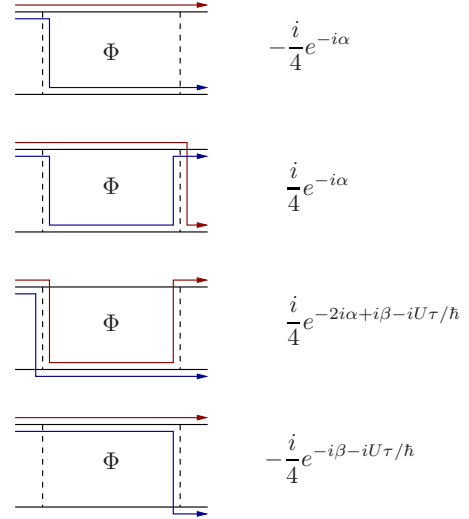

FIG. 5. (Color online) As in Fig. 4 but with one particle on the lower channel in the final state. The combined amplitude is $A_1 = -\frac{1}{2}e^{-i\alpha}e^{-iU\tau/\hbar}\sin\Phi$.

simply be a product of contributions for each particle. Interactions contribute additional phase factors $e^{-iU\tau/\hbar}$ when both particles propagate on the same channel inside the interferometer. The average charge transferred between the upper and lower channels in the scattering process is

$$I = 2|A_2|^2 + 2|A_1|^2 = 1 + \cos(U\tau/\hbar)\cos\Phi, \qquad (1)$$

where both terms are multiplied by factors of two since A_2 describes two-particle transmission while single-particle transmission with amplitude A_1 can occur for either particle. AB oscillations are represented in this expression by the term in $\cos\Phi$. Their strength is modulated by the factor $\cos(U\tau/\hbar)$. We can take the interaction strength U to play the same role in the two-particle problem as bias voltage in the many-body system since increasing bias leads to reduced spatial separation between electrons entering the MZI above a filled Fermi sea, which in turn increases the interaction energy between these electrons.

The phenomenon can be summarized by defining the visibility of AB oscillations. Let I_{max} and I_{min} be the maximum and minimum values of I as Φ varies. The visibility is

$$\mathcal{V} = \frac{I_{max} - I_{min}}{I_{max} + I_{min}}. \qquad (2)$$

From Eq. (1) we have $\mathcal{V} = |\cos(U\tau/\hbar)|$ and hence a lobe pattern in $\mathcal{V}$ as a function of U. It is also evident from Eq. (1) that the phase of AB oscillations changes abruptly by π at zeros of $\mathcal{V}$.

We use the same approach to calculate the current for the case of arbitrary tunneling amplitudes t_a, t_b at the QPCs. The result for the average charge transferred is

$$I = 2\{T_aR_b + R_aT_b + 2(T_aT_bR_aR_b)^{1/2}$$
$$\times [1 - 4(T_aR_a)\sin^2(U\tau/\hbar)]^{1/2}\cos\tilde{\Phi}\}, \qquad (3)$$

where $T_{a,b} = 1 - R_{a,b} = t_{a,b}^2$ is the tunneling probability. The phase of AB oscillations is shifted by interactions, being
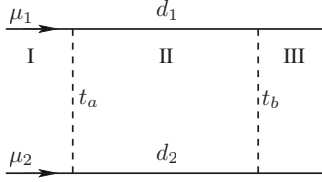
FIG. 6. Schematic view of the MZI. Horizontal lines represent edge states with propagation direction indicated by arrows. These edge states are connected by two QPCs, shown as vertical dashed lines, with tunneling amplitudes t_a and t_b. The arm lengths between contacts are d_1 and d_2, and the chemical potentials in the incident channels are μ_1 and μ_2. The three different regions of the interferometer discussed in the text are labeled using Roman numerals.

$$\widetilde{\Phi} = \Phi + \arccos\{[1 - 4(T_a R_a)\sin^2(U\tau/\hbar)]^{-1/2}\cos(U\tau/\hbar)\}. \tag{4}$$

The visibility is

$$\mathcal{V} = \mathcal{V}_0 \times [1 - 4(T_a R_a)\sin^2(U\tau/\hbar)]^{1/2}, \tag{5}$$

where $\mathcal{V}_0$ is the single-particle value

$$\mathcal{V}_0 = \frac{2[T_a T_b R_a R_b]^{1/2}}{T_a R_b + R_a T_b}. \tag{6}$$

An important difference between these results and the ones for the many-body problem that we present in Sec. V is that here $\mathcal{V}$ does not decay at large U. In other respects, however, the two-body problem is illuminating. In particular, while the behavior of $\mathcal{V}$ is not affected by the value of T_b except for a multiplicative factor, if $T_a \neq 1/2$ the zeros of the visibility turn into finite minima and the jumps in the phase of AB oscillations become smooth rises. In the limit that transmission at the first QPQ approaches $T_a=1$ or $T_a=0$, modulations of $\mathcal{V}$ with U disappear altogether. These features are also present in the many-body problem. One consequence is that the lobe pattern cannot be obtained at leading order from a calculation that is perturbative in tunneling.

III. MICROSCOPIC MODEL OF THE MZI

Our model for the MZI is sketched in Fig. 6. The Hamiltonian is

$$\hat{\mathcal{H}} = \hat{\mathcal{H}}_{kin} + \hat{\mathcal{H}}_{tun} + \hat{\mathcal{H}}_{int}. \tag{7}$$

It has three contributions: $\hat{\mathcal{H}}_{kin}$ is the single-particle term for an isolated edge; $\hat{\mathcal{H}}_{int}$ represents electron-electron interactions; and $\hat{\mathcal{H}}_{tun} = \hat{\mathcal{H}}^a_{tun} + \hat{\mathcal{H}}^b_{tun}$ describes tunneling at the QPCs labeled a and b. We consider initially edge channels of length L with periodic boundary conditions, then take $L \to \infty$. Allowed wave vectors are $k = 2\pi n_k/L$ with n_k integer. Fermionic operators $\hat{c}^+_{k\eta}$ and $\hat{c}_{k\eta}$, which create and annihilate an electron with momentum k on the edge η, obey standard anticommutation relations $\{\hat{c}_{k\eta}, \hat{c}^+_{p\eta'}\} = \delta_{kp}\delta_{\eta\eta'}$. In coordinate representation the field operator $\hat{\psi}_\eta(x)$, which annihilates an electron at position x on the edge η, is

$$\hat{\psi}_\eta(x) = \frac{1}{\sqrt{L}}\sum_{k=-\infty}^{\infty}\hat{c}_{k\eta}e^{ikx}. \tag{8}$$

With this notation

$$\hat{\mathcal{H}}_{kin} = -i\hbar v_F\sum_{\eta=1,2}\int_{-L/2}^{L/2}\hat{\psi}^+_\eta(x)\partial_x\hat{\psi}_\eta(x)dx. \tag{9}$$

We represent interactions within each edge using the same symmetric potential $U(x,x')$ and neglect interactions between electrons in different edges. Introducing the density operator $\hat{\rho}_\eta(x) = \hat{\psi}^+_\eta(x)\hat{\psi}_\eta(x)$, we then have

$$\hat{\mathcal{H}}_{int} = \frac{1}{2}\sum_{\eta=1,2}\int_{-L/2}^{L/2}U(x,x')\hat{\rho}_\eta(x)\hat{\rho}_\eta(x')dxdx'. \tag{10}$$

Finally, taking the QPCs to be pointlike, we write

$$\hat{\mathcal{H}}^a_{tun} = v_a e^{i\alpha}\hat{\psi}^+_1(0)\hat{\psi}_2(0) + \text{H.c.}, \tag{11}$$

$$\hat{\mathcal{H}}^b_{tun} = v_b e^{i\beta}\hat{\psi}^+_1(d_1)\hat{\psi}_2(d_2) + \text{H.c.} \tag{12}$$

Here v_a and v_b are tunneling strengths, from which the quantum amplitudes t_a and t_b can be calculated. As in the previous section, the AB phase due to enclosed flux is $\Phi = \beta - \alpha$.

This model can be solved exactly when interactions occur only between pairs of electrons that are both inside the interferometer, in the region denoted II in Fig. 6. We present results in Sec. V calculated using three different choices for such internal interactions. The first of these is simply a charging energy

$$U(x,x') = \begin{cases} g & 0 < x,x' < d \\ 0 & \text{otherwise}. \end{cases} \tag{13}$$

An interaction of this kind is standard in the theory of quantum dots and for an MZI was treated approximately in Ref. 32. To test the robustness of behavior to changes in the form of interaction, we also obtain results for two types of interaction potential that vary with electron separation inside the interferometer, taking

$$U(x,x') = \begin{cases} U(x-x') & 0 < x,x' < d \\ 0 & \text{otherwise} \end{cases} \tag{14}$$

and either an exponential dependence

$$U(x-x') = ge^{-\alpha|x-x'|} \tag{15}$$

or a Coulomb form

$$U(x-x') = \frac{g_c}{\sqrt{(x-x')^2 + a_c^2}}. \tag{16}$$

IV. EXACT SOLUTION

In this section we give a full account of the solution outlined previously in Ref. 34. We study the interferometer at finite bias voltage by computing the quantum-mechanical time evolution of an initial state in which the single-particle

levels of $\hat{\mathcal{H}}_{kin}$ for the two edges are occupied up to different chemical potentials, μ_1 and μ_2. The interferometer reaches a steady state at long times and we evaluate observables in this state. The challenge of the calculation comes from the difficulty of treating both tunneling and interactions nonperturbatively. Each part of the problem can be described by a quadratic Hamiltonian but the appropriate variables are different in the two cases: fermionic for tunneling and bosonic for interactions. A model which has only internal interactions can be solved exactly because in these circumstances the effects of tunneling at QPCs and of interactions can be handled separately. In the following we consider only edge states at filling factor $\nu=1$ and an initial state at zero temperature but both these restrictions could be lifted within the approach.

To treat time evolution we use the interaction representation, taking as the free part of the Hamiltonian

$$\hat{H}_0 = \hat{\mathcal{H}}_{kin} + \hat{\mathcal{H}}_{int} \qquad (17)$$

and as the "interaction" part $\hat{\mathcal{H}}_{tun}$. In this representation the time evolution of the fermion operators is given by

$$\hat{\psi}_\eta(x,t) = e^{i\hat{H}_0 t/\hbar} \hat{\psi}_\eta(x) e^{-i\hat{H}_0 t/\hbar}. \qquad (18)$$

The wave function of the system, which we denote at $t=0$ by $|Fs\rangle$, evolves with the S matrix

$$\hat{S}(t) = T \exp\left\{ -\frac{i}{\hbar} \int_0^t \hat{\mathcal{H}}_{tun}(\tau) d\tau \right\}, \qquad (19)$$

where T denotes time ordering. We distinguish operators in the Schrödinger and interaction representations by the absence or presence of a time argument. In Sec. IV A we also use operators in the Heisenberg representation and we indicate these with a subscript H.

The presentation of the remainder of the calculation is organized as follows. The observable we are concerned with is the current through the MZI and we derive a convenient form for the corresponding operator in Sec. IV A. The simplifications arising in a model with only internal interactions affect the calculation of the S matrix of Eq. (19), which we describe in Sec. IV B. To find the time evolution of fermion operators we use bosonization, as set out in Sec. IV C. After bosonization $\hat{H}_0$ is quadratic and may either be treated using scattering theory (Sec. IV D) or diagonalized using a Bogoliubov transformation (Sec. IV E). Inverting our transformations, we arrive in Sec. IV F at an expression for current at long times, written in terms of fermion operators in the Schrödinger picture, and show that this expression is suitable for numerical evaluation. We give results for different choices of interaction potential in Sec. V.

A. Derivation of the current operator

Although it is usual to write $\hat{\mathcal{H}}_{tun}$ as in Eqs. (11) and (12), this is a shorthand since at finite tunneling strength the fermion field is discontinuous at QPCs. For that reason we regularize $\hat{\mathcal{H}}_{tun}$ by considering QPCs of finite extent w, tak-

ing $w \to 0$ at the end of calculations. Then, for example, $\hat{\mathcal{H}}_{tun}^b$ has the form

$$\hat{\mathcal{H}}_{tun}^b = \frac{1}{w} \int_0^w dx [v_b e^{i\beta} \hat{\psi}_1^+(d_1 + x) \hat{\psi}_2(d_2 + x) + \text{H.c.}]. \quad (20)$$

The current operator can be found in the standard way from the number operator $\hat{N}_1 = \int \hat{\rho}_1(x) dx$ for electrons on the upper edge, by evaluating its commutator with $\hat{\mathcal{H}}$. This gives for the current at QPC b

$$\hat{I}_b = -\frac{2e}{w\hbar} \Im \int_0^w v_b e^{i\beta} \hat{\psi}_1^+(d_1 + x) \hat{\psi}_2(d_2 + x) dx \qquad (21)$$

and a similar expression for $\hat{I}_a$, the current at QPC a. To calculate the position dependence of fermion fields within the QPCs we introduce operators in the Heisenberg representation with the time dependence

$$\hat{A}_H(t) = e^{i\hat{\mathcal{H}} t/\hbar} \hat{A} e^{-i\hat{\mathcal{H}} t/\hbar}. \qquad (22)$$

The equations of motion for the fermion operators at the contact b have in the interval $0 \le x \le w$ the form

$$(\partial_t + v_F \partial_x) \hat{\psi}_{1H}^+(d_1 + x, t) = i \frac{v_b}{w} e^{-i\beta} \hat{\psi}_{2H}^+(d_2 + x, t),$$

$$(\partial_t + v_F \partial_x) \hat{\psi}_{2H}^+(d_2 + x, t) = i \frac{v_b}{w} e^{i\beta} \hat{\psi}_{1H}^+(d_1 + x, t).$$

This system of equations has in the same interval the solution

$$\hat{\psi}_{\eta H}^+(d_\eta + x, t) = \sum_{\eta'=1,2} M_{\eta\eta'} \hat{\psi}_{\eta'H}^+(d_{\eta'}, t - x/v_F), \quad (23)$$

where $M = \exp(ix\Sigma)$ and the matrix Σ is

$$\Sigma = \frac{v_b}{wv_F} \begin{pmatrix} 0 & e^{-i\beta} \\ e^{i\beta} & 0 \end{pmatrix}.$$

An explicit expression for the matrix M is

$$M = \begin{bmatrix} \cos\theta(x) & ie^{-i\beta}\sin\theta(x) \\ ie^{i\beta}\sin\theta(x) & \cos\theta(x) \end{bmatrix}$$

with $\theta(x) = xv_b/wv_F\hbar$. Taking the limit $w \to 0$ and writing $\varepsilon = +0$, we arrive at a relation between fermion operators at $d_\eta + \varepsilon$, just after the tunneling contact b, and those at $d_{\eta'} - \varepsilon$, just before the contact

$$\hat{\psi}_{\eta H}^+(d_\eta + \varepsilon, t) = \sum_{\eta'=1,2} \mathcal{S}_{\eta\eta'}^{(b)*} \hat{\psi}_{\eta'H}^+(d_{\eta'} - \varepsilon, t) \qquad (24)$$

with the scattering matrix

$$\mathcal{S}^{(b)} \equiv \begin{pmatrix} r_b & -it_b e^{i\beta} \\ -it_b e^{-i\beta} & r_b \end{pmatrix}. \qquad (25)$$

In this way the reflection $r_{a,b} = \cos\theta_{a,b}$ and transmission $t_{a,b} = \sin\theta_{a,b}$ amplitudes at the contact a, b are expressed in terms of the angles $\theta_{a,b} = v_{a,b}/\hbar v_F$.

Substitution of Eq. (23) into Eq. (21) and reversion to the Schrödinger picture gives for the current operator $\hat{I}_b$ the result

$$\hat{I}_b = ev_F\{t_b^2[\hat{\rho}_{1H}(d_1 - \varepsilon) - \hat{\rho}_{2H}(d_2 - \varepsilon)] + t_b r_b$$
$$\times[ie^{i\beta}\hat{\psi}_{1H}^+(d_1 - \varepsilon)\hat{\psi}_{2H}(d_2 - \varepsilon) + \text{H.c.}]\} \quad (26)$$

in which we show explicitly that all operators are evaluated at a point infinitesimally before the contact. In the following we will omit ε. An expression for the current operator at QPC a is obtained from Eq. (26) by substituting 0 for $d_{1,2}$ and replacing θ_b with θ_a. The total current operator is then $\hat{I} = \hat{I}_a + \hat{I}_b$.

When considering expectation values, denoted by $\langle \ldots \rangle$ or by omitting hats, it is useful to separate the contribution from QPC b into two terms, $I_b = I_b^{(1)} + I_b^{(2)}$, with

$$I_b^{(1)} = ev_F t_b^2\langle\hat{\rho}_1(d_1) - \hat{\rho}_2(d_2)\rangle,$$

$$I_b^{(2)} = ev_F t_b r_b[ie^{i\beta}\langle\hat{G}_{12}\rangle + \text{H.c.}], \quad (27)$$

where $\hat{G}_{12} = \hat{\psi}_1^+(d_1)\hat{\psi}_2(d_2)$. The term $I_b^{(2)}$ is sensitive to the coherence between edges while $I_b^{(1)}$ is insensitive. Since there is no coherence between channels before contact a, $I_a^{(2)} = 0$ and the contribution to the current from this contact is

$$I_a^{(1)} = ev_F t_a^2\langle\hat{\rho}_1(0) - \hat{\rho}_2(0)\rangle. \quad (28)$$

The term responsible for AB fringes in the current is $I_b^{(2)}$ and our general task is to calculate $\langle\hat{G}_{12}\rangle$.

In experiment the differential conductance $\mathcal{G} = edI/d\mu_1$ (with μ_2 fixed) is measured at finite bias voltage $V = (\mu_1 - \mu_2)/e$. $\mathcal{G}$ oscillates with Φ, having maximum and minimum values $\mathcal{G}_{max}$ and $\mathcal{G}_{min}$. The AB *fringe visibility* is defined as

$$\mathcal{V} = \frac{\mathcal{G}_{max} - \mathcal{G}_{min}}{\mathcal{G}_{max} + \mathcal{G}_{min}}. \quad (29)$$

B. Evaluation of the S matrix

We require the action of the S matrix, Eq. (19), on the initial state $|Fs\rangle$. This state is represented by a product of fermion creation operators acting on the vacuum and we need to find how $\hat{S}(t)$ transforms the fermion operators. Evaluation of $\hat{S}(t)$ is based on our restriction of interactions to the interior of the MZI. Specifically, separating $\hat{\mathcal{H}}_{tun}$ into parts $\hat{\mathcal{H}}_{tun}^a$ and $\hat{\mathcal{H}}_{tun}^b$ due to each QPC, we find (see Appendix A) that

$$[\hat{\mathcal{H}}_{tun}^a(t_1), \hat{\mathcal{H}}_{tun}^b(t_2)] = 0 \quad (30)$$

for $t_1 \geq t_2$. This leads to a factorization of the S matrix into the product $\hat{S}(t) = \hat{S}^b(t)\hat{S}^a(t)$, where $\hat{S}^a(t)$ is the S matrix calculated using $\hat{\mathcal{H}}_{tun}^a$, and $\hat{S}^b(t)$ using $\hat{\mathcal{H}}_{tun}^b$. A second commutator (see again Appendix A)

$$[\hat{G}_{12}(t_1), \hat{\mathcal{H}}_{tun}^b(t_2)] = 0$$

also valid for $t_1 \geq t_2$, ensures that

$$[\hat{S}^b(t)]^+\hat{G}_{12}(t)\hat{S}^b(t) = \hat{G}_{12}(t) \quad (31)$$

so an explicit form for $\hat{S}^b(t)$ is not required in the calculation. Since QPC a acts before the interacting region, it is easy to evaluate $\hat{S}^a(t)$ (Appendix B): we have

$$[\hat{\mathcal{H}}_{tun}^a(t_1), \hat{\mathcal{H}}_{tun}^a(t_2)] = 0$$

for any t_1, $t_2 \geq 0$ and so may omit time ordering. The action of $\hat{S}^a(t)$ on fermionic operators is a rotation in the space of channels and can be written as

$$\tilde{\hat{\psi}}_\eta(x) = [\hat{S}^a(t)]^+\hat{\psi}_{\eta'}(x)\hat{S}^a(t). \quad (32)$$

For $0 < x < v_F t$ we find the transformation

$$\tilde{\hat{\psi}}_\alpha(x) = \sum_\beta \mathcal{S}_{\alpha\beta}^a\hat{\psi}_\beta(x) \quad (33)$$

with the rotation matrix given by

$$\mathcal{S}^a = \begin{pmatrix} r_a & -it_a e^{i\alpha} \\ -it_a e^{-i\alpha} & r_a \end{pmatrix}. \quad (34)$$

C. Bosonization

To compute the time evolution of operators in the interaction representation under $\hat{H}_0$ we use bosonization.[35] This gives us an exact correspondence between fermion and boson operators via the bosonization identity

$$\hat{\psi}_\eta(x) = (2\pi a)^{-1/2}\hat{F}_\eta e^{i(2\pi/L)\hat{N}_\eta x}e^{-i\hat{\phi}_\eta(x)}, \quad (35)$$

where bosonic fields are defined as

$$\hat{\phi}_\eta(x) = -\sum_{q>0}(2\pi/qL)^{1/2}(e^{iqx}\hat{b}_{q\eta} + \text{H.c.})e^{-qa/2} \quad (36)$$

and a is an infinitesimal regulator, which does not enter the final results. The plasmon creation and annihilation operators (which have $q > 0$) obey bosonic commutation relations

$$[\hat{b}_{q\eta}, \hat{b}_{k\eta'}^+] = \delta_{qk}\delta_{\eta\eta'}. \quad (37)$$

They can be expressed in terms of fermions as

$$\hat{b}_{q\eta}^+ = i(2\pi/qL)^{1/2}\sum_{k=-\infty}^{\infty}\hat{c}_{k+q\eta}^+\hat{c}_{k\eta}. \quad (38)$$

The commutation relations for the fields $\hat{\phi}_\eta(x)$ (omitting terms proportional to $1/L$: see discussion in Ref. 35) read

$$[\hat{\phi}_\eta(x), \partial_y\hat{\phi}_{\eta'}(y)] = -2\pi i\delta(x - y)\delta_{\eta\eta'}.$$

The Klein factors $\hat{F}_\eta$ which change fermion number by one, satisfy the commutation relations

$$\{\hat{F}_\eta, \hat{F}_{\eta'}^+\} = 2\delta_{\eta\eta'}, [\hat{N}_\eta, \hat{F}_{\eta'}] = -\delta_{\eta\eta'}\hat{F}_\eta$$

with the standard expression for the particle number operator

$$\hat{N}_\eta \equiv \sum_{k=-\infty}^{\infty} \hat{c}_{k\eta}^+ \hat{c}_{k\eta} - \sum_{k=-\infty}^{\infty} \langle 0|\hat{c}_{k\eta}^+ \hat{c}_{k\eta}|0\rangle \qquad (39)$$

in the edge η. Here the vacuum state $|0\rangle$ satisfies

$$\hat{c}_{k\eta}^+ |0\rangle \equiv 0, \quad k \leq 0,$$

$$\hat{c}_{k\eta}|0\rangle \equiv 0, \quad k > 0.$$

The commutators $[F_\eta, \hat{b}_{k\eta'}]$ and $[\hat{N}_\eta, \hat{b}_{k\eta'}]$ are zero. The electron-density operator is given by

$$\hat{\rho}_\eta(x) = -\frac{1}{2\pi}\partial_x \hat{\phi}_\eta(x) + \hat{N}_\eta/L. \qquad (40)$$

Since $\hat{H}_0$ does not couple channels, in the following we restrict our attention to a single channel and omit channel labels until we reach Sec. IV F. The kinetic energy $\hat{\mathcal{H}}_{kin}$ for a single edge in bosonized form is

$$\hat{\mathcal{H}}_{kin} = \frac{\hbar v_F}{2} \int_{-L/2}^{L/2} \frac{dx}{2\pi}[\partial_x \hat{\phi}(x)]^2 + \frac{2\pi}{L}\frac{\hbar v_F}{2}\hat{N}(\hat{N}+1). \qquad (41)$$

Similarly, $\hat{\mathcal{H}}_{int}$ is quadratic, and given by

$$\hat{\mathcal{H}}_{int} = \frac{1}{2}\int_0^d \int_0^d U(x,x')\hat{\rho}(x)\hat{\rho}(x')dxdx'. \qquad (42)$$

Using this form of the Hamiltonian, our objective is to express the time-dependent boson field $\hat{\phi}(d,t)$ in the interaction representation, in terms the boson operators $\hat{b}_q$ and $\hat{b}_q^+$ in the Schrödinger representation. We set out two approaches to this calculation. One is based on the formalism of scattering theory. We use this to treat interactions for which we can obtain simple expressions for plasmon scattering phase shifts. The other is based on a Bogoliubov transformation. We use it to study Coulomb interactions.

D. Scattering approach

The theory of plasmon scattering in spatially inhomogeneous systems of quantum-Hall-edge channels has been studied quite extensively. An early treatment of a Hall bar is given in Ref. 36 and a recent application to an MZI is described in Ref. 29. For the model we are concerned with, consider the equation of motion

$$i\hbar\partial_t \hat{\phi}(x,t) = [\hat{\phi}(x,t),\hat{H}_0]. \qquad (43)$$

We separate $\hat{\phi}(x,t) = \hat{\phi}^{(0)}(x,t) + \hat{\phi}^{(1)}(x,t)$ into a part $\hat{\phi}^{(0)}(x,t)$, proportional to $\hat{N}$, and another part $\hat{\phi}^{(1)}(x,t)$, independent of $\hat{N}$. They obey

$$i\hbar\partial_t \hat{\phi}^{(0)}(x,t) = -i\hbar v_F \partial_x \hat{\phi}^{(0)}(x,t) + i\frac{\hat{N}}{L}\int_0^d U(x,y)dy$$

$$- \frac{i}{2\pi}\int_0^d U(x,y)\partial_y \hat{\phi}^{(0)}(y,t)dy \qquad (44)$$

and

$$i\hbar\partial_t \hat{\phi}^{(1)}(x,t) = -i\hbar v_F \partial_x \hat{\phi}^{(1)}(x,t) - \frac{i}{2\pi}\int_0^d U(x,y)\partial_y \hat{\phi}^{(1)}(y,t)dy \qquad (45)$$

with initial conditions $\hat{\phi}^{(0)}(x,0)=0$ and $\hat{\phi}^{(1)}(x,0)=\hat{\phi}(x)$. Our aim is to find the Green's function for Eq. (45).

The basis functions for a mode expansion of $\hat{\phi}^{(1)}(x,t)$ obey the time-independent Schrödinger equation

$$\omega_p f_p(x) = -iv_F \partial_x f_p(x) - \frac{i}{2\pi\hbar}\int_0^d U(x,y)\partial_y f_p(y) \qquad (46)$$

and satisfy the orthonormality relation

$$\int_{-L/2}^{L/2} f_p(x)\partial_x f_q^*(x)dx = -2\pi i \delta_{pq}. \qquad (47)$$

The Green's function can therefore be written as

$$K(x,y;t) = \frac{i}{2\pi}\sum_p f_p(x)\partial_y f_p^*(y)e^{-i\omega_p t} \qquad (48)$$

and we have

$$\hat{\phi}^{(1)}(x,t) = \int_{-L/2}^{L/2} K(x,y;t)\hat{\phi}(y)dy. \qquad (49)$$

Interactions within the MZI generate a frequency-dependent phase shift δ_p for plasmons and the form of $f_p(x)$ on either side of the interaction region is (neglecting a correction to the normalization that vanishes as $d/L\to 0$)

$$f_p(x) = -\left(\frac{2\pi}{qL}\right)^{1/2}\begin{cases} e^{iqx} & x \leq 0 \\ e^{i(qx-\delta_q)} & x \geq d. \end{cases}$$

With periodic boundary conditions at finite L, the allowed values of q are fixed by the condition $f_p(-L/2)=f_p(L/2)$, and these determine the frequencies $\omega_p=v_F q$. At long times and for large L, the quantity we require, $K(d,y;t)$, can be expressed solely in terms of these phase shifts as

$$K(d,y;t) = \frac{1}{2\pi}\int_{-\infty}^{\infty} dp\, e^{i(p[d-y-v_F t]-\delta_p)}. \qquad (50)$$

From this we obtain

$$\hat{\phi}^{(1)}(x,t) = \sum_{q>0}[z_q(x,t)\hat{b}_q + \text{H.c.}] \qquad (51)$$

in which the coefficients at long times have the form

$$z_q(d,t) = -(2\pi/qL)^{1/2}e^{iq(d-v_F t)-i\delta_q}. \qquad (52)$$

The long time limit of $\hat{\phi}^{(0)}(d,t)$, which we write as $\hat{\phi}_0(d)$, can also be expressed in terms of the phase shifts, as

$$\hat{\phi}_0(d) = 2\pi\frac{\hat{N}}{L}\lim_{q\to 0}\frac{\delta_q}{q}. \qquad (53)$$

E. Diagonalization by Bogoliubov transformation

An alternative approach is to diagonalize the Hamiltonian. Substituting Eq. (36) into $\hat{H}_0$ we obtain

$$\hat{H}_0 = \hbar v_F \sum_{q>0} q(\hat{b}_q^+ \hat{b}_q + 1/2) + \frac{\hbar}{2L} \sum_{k,q>0} \sqrt{qk}[u_{-q,-k}\hat{b}_q\hat{b}_k^+$$
$$+ u_{q,k}\hat{b}_q^+\hat{b}_k - u_{q,-k}\hat{b}_q^+\hat{b}_k^+ - u_{-q,k}\hat{b}_q\hat{b}_k] + \hat{H}_{N\phi} + \hat{H}_N, \tag{54}$$

where the matrix elements of the interaction potential are

$$u_{q,k} = \frac{1}{2\pi\hbar} \int_0^d \int_0^d e^{-iqx+iky} U(x,y)dxdy. $$

They obey the relations $u_{q,k}^* = u_{-q,-k}$ and $u_{q,k} = u_{-k,-q}$.

The last two terms in Eq. (54) involve the number operator $\hat{N}$. The first of them appears because of our choice of nonuniform interactions, which leads to a coupling

$$\hat{H}_{N\phi} = i\hbar(\hat{N}/L)(2\pi/L)^{1/2} \sum_{k>0} \sqrt{k}[u_{0,k}\hat{b}_k - u_{0,-k}\hat{b}_k^+] \tag{55}$$

between the plasmon and the number operators: by contrast, in a system with translationally invariant interactions there would be no such coupling. The other term, $\hat{H}_N$, has the form

$$\hat{H}_N = \frac{2\pi}{L}\frac{\hbar v_F}{2}\hat{N}(\hat{N}+1) + \frac{\hat{N}^2}{2L^2}\int_0^d U(x,x')dxdx'. \tag{56}$$

Since interactions in our model are limited to the finite region of length d, the second term in Eq. (56) gives a correction to, for example, the equation of motion of the Klein factor that is small in d/L and so vanishes in the thermodynamic limit. We therefore omit it in the following.

Contributions to the Hamiltonian linear in $\hat{N}$ are removed by making the shifts

$$\hat{b}_q = \tilde{b}_q + \alpha_q \hat{N} \tag{57}$$

with coefficients α_q given by

$$v_F\alpha_q + \frac{1}{L}\sum_{k>0}\sqrt{k/q}[u_{qk}\alpha_k - u_{q,-k}\alpha_k^*] = \frac{i}{L}\left(\frac{2\pi}{qL}\right)^{1/2}u_{q0}. \tag{58}$$

The Hamiltonian, Eq. (54), written in terms of these shifted operators, is diagonalized using a Bogoliubov transformation of the form

$$\hat{\beta}_p^+ = \sum_{q>0}(A_{pq}\tilde{b}_q^+ + B_{pq}\tilde{b}_q). \tag{59}$$

To preserve the commutation relations we require

$$\sum_{k>0}(A_{pk}A_{kq}^+ - B_{pk}B_{kq}^+) = \delta_{pq}, \tag{60}$$

$$\sum_{k>0}(B_{pk}A_{kq}^T - A_{pk}B_{kq}^T) = 0, \tag{61}$$

which can be written in the matrix form

$$\begin{pmatrix} A & B \\ B^* & A^* \end{pmatrix}\begin{pmatrix} A^+ & -B^T \\ -B^+ & A^T \end{pmatrix} = \begin{pmatrix} I & 0 \\ 0 & I \end{pmatrix}, \tag{62}$$

where I is the identity matrix.

The result is

$$\mathcal{H}_b = \sum_{p>0}\hbar\omega_p(\hat{\beta}_p^+\hat{\beta}_p + 1/2) + \hat{H}_N + \text{const.} \tag{63}$$

The time dependence of the transformed boson operators is given in the usual way in terms of their frequencies ω_p as $\hat{\beta}_p(t) = e^{-i\omega_p t}\hat{\beta}_p$. Expressions for the coefficients A_{pq}, B_{pq} can be found from the commutator

$$\partial_t\hat{\beta}_q = -i[\hat{\beta}_q, \hat{\mathcal{H}}_b] = -i\hbar\omega_q\hat{\beta}_q, \tag{64}$$

which leads to the linear system of Bogoliubov equations

$$(\omega_p - v_F q)A_{pq} = \sum_{k>0}\sqrt{qk}[u_{qk}A_{pk} + u_{q,-k}B_{pk}],$$

$$(\omega_p + v_F q)B_{pq} = -\sum_{k>0}\sqrt{qk}[u_{-q,k}A_{pk} + u_{-q,-k}B_{pk}]. \tag{65}$$

From Eq. (62) we can obtain the inverse of the Bogoliubov transformation, which we write in the interaction representation as

$$\tilde{b}_q^+(t) = \sum_{p>0}(\hat{\beta}_p^+ e^{i\omega_p t}A_{pq}^* - \hat{\beta}_p e^{-i\omega_p t}B_{pq}). \tag{66}$$

Substituting Eqs. (57) and (59) into Eq. (66) we obtain the time dependence of the bosonic fields in terms of the original operators $\hat{b}_q$ written in the Schrödinger representation as

$$\hat{\phi}(x,t) = \hat{\phi}^{(0)}(x,t) + \sum_{q>0}[z_q(x,t)\hat{b}_q + \text{H.c.}], \tag{67}$$

where

$$z_q(x,t) = \sum_{p>0}[A_{pq}^* f_p(x)e^{-i\omega_p t} + B_{pq}f_p^*(x)e^{i\omega_p t}] \tag{68}$$

with

$$f_p(x) = -\sum_{q>0}(2\pi/qL)^{1/2}(A_{pq}e^{iqx} - B_{pq}e^{-iqx}). \tag{69}$$

The term $\hat{\phi}^{(0)}(x,t)$ in Eq. (67), arising from the operator shifts, is given by

$$\hat{\phi}^{(0)}(x,t) = \hat{\phi}_0(x) - \hat{N}\sum_{q>0}[z_q(x,t)\alpha_q + \text{c.c.}] \tag{70}$$

with

$$\hat{\phi}_0(x) = -\hat{N}\sum_{q>0}(2\pi/qL)^{1/2}(\alpha_q e^{iqx} + \text{c.c.}).$$

It is easy to check that at $t=0$ the field in Eq. (67) is equal to the Schrödinger operator $\hat{\phi}(x)$ of Eq. (35) since $z_q(x,0) = -(2\pi/qL)^{1/2}e^{iqx}$ and $\hat{\phi}^{(0)}(x,0) = 0$.

To make use of these results, the Bogoliubov coefficients A_{pq}, B_{pq}, and α_q, and frequencies ω_p are required. They can be found from Eqs. (58) and (65), using a numerical treatment with a momentum cutoff.

F. Evaluation of the correlators

In this section we explain how the treatment we have described of the bosonized Hamiltonian enables evaluation

of the correlator $\hat{G}_{12}(t)$, which appears in Eq. (27) and determines visibility of AB oscillations. When written using fermion fields in the interaction representation, it is

$$\hat{G}_{12} = \langle Fs|[\hat{S}^a(t)]^+\hat{\psi}_1^+(d_1,t)\hat{\psi}_2(d_2,t)\hat{S}^a(t)|Fs\rangle. \quad (71)$$

Our objective is to express $\hat{\psi}_1^+(d_1,t)$ and $\hat{\psi}_2(d_2,t)$ in terms fermion fields $\hat{\psi}_\eta(x)$ and $\hat{\psi}_\eta^+(x)$ in the Schrödinger representation so that the expectation value in the state $|Fs\rangle$ can be computed. To this end we use the bosonization identity, Eq. (35), and simplify notation by defining

$$\hat{\mathcal{F}}_\eta(t) \equiv (2\pi a)^{-1/2}e^{i\hat{H}_0 t}\hat{F}_\eta e^{i(2\pi/L)\hat{N}_\eta d_\eta}e^{-i\hat{H}_0 t}. \quad (72)$$

Then

$$\hat{\psi}_\eta(d_\eta,t) = \hat{\mathcal{F}}_\eta(t)e^{-i\hat{\phi}_\eta(d_\eta,t)}. \quad (73)$$

The bosonic field $\phi_\eta(d_\eta,t)$ which appears here in the interaction representation is related at long times to one in the Schrödinger representation by Eqs. (52) and (53). In addition, the time evolution of the operator $\hat{\mathcal{F}}_\eta(t)$ can be found in the usual way, via its commutator with $\hat{H}_0$ (the contribution from $\hat{H}_{N\phi}$ is small in d/L and can be omitted in the thermodynamic limit), giving

$$\hat{\mathcal{F}}_\eta(t) = (2\pi a)^{-1/2}\hat{F}_\eta e^{i(2\pi/L)\hat{N}_\eta(d_\eta - v_F t)}. \quad (74)$$

We wish to substitute for the Klein factor $\hat{F}_\eta$ in this expression. Consider a fermionic operator $\hat{\psi}_\eta(z_\eta)$ with $z_\eta = d_\eta - v_F t$. In the bosonized form, from Eq. (35) it is

$$\hat{\psi}_\eta(z_\eta) = (2\pi a)^{-1/2}\hat{F}_\eta e^{i(2\pi/L)\hat{N}_\eta(d_\eta - v_F t)}e^{-i\hat{\phi}_\eta(z_\eta)}. \quad (75)$$

Multiplying Eq. (75) by $e^{i\hat{\phi}_\eta(z_\eta)}$ from the right we obtain $\mathcal{F}_\eta(t)$ in terms of the fermion operators and bosonic fields in their Schrödinger representation, as

$$\hat{\mathcal{F}}_\eta(t) = \hat{\psi}_\eta(z_\eta)e^{i\hat{\phi}_\eta(z_\eta)} = e^{i\hat{\phi}_\eta(z_\eta)}\hat{\psi}_\eta(z_\eta), \quad (76)$$

where the second equality holds due to the commutation relations of Klein factors with bosonic operators. Substituting Eq. (76) into Eq. (73) we obtain

$$\hat{\psi}_\eta(d_\eta,t) = e^{-i\hat{\phi}_\eta(d_\eta t)}e^{i\hat{\phi}_\eta(z_\eta)}\hat{\psi}_\eta(z_\eta), \quad (77)$$

which can be written as

$$\hat{\psi}_\eta(d_\eta,t) = e^{-i\varphi_\eta}e^{-i[\hat{\phi}_\eta(d_\eta t) - \hat{\phi}_\eta(z_\eta)]}\hat{\psi}_\eta(z_\eta), \quad (78)$$

where the constant phase shift φ_η is given by

$$\varphi_\eta = \frac{i}{2}\int \frac{dq}{q}e^{-i\delta_{q\eta}}. \quad (79)$$

Finally, we substitute for $\hat{b}_{q\eta}$ and $\hat{b}_{q\eta}^+$ in $\hat{\phi}_\eta(x)$ in terms of fermion operators, using Eq. (38), with the result

$$\hat{\psi}_\eta(d_\eta,t) = e^{-i\varphi_\eta}e^{-i\hat{Q}_\eta}\hat{\psi}_\eta(z_\eta). \quad (80)$$

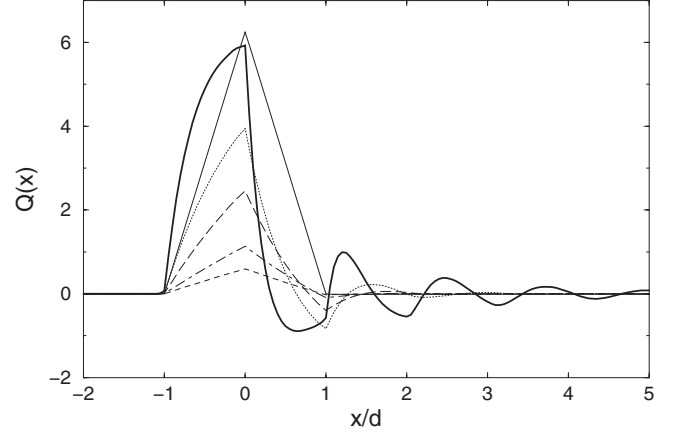Here the phase operator $\hat{Q}_\eta$ is

FIG. 7. The kernel $Q(x)$ of Eq. (81) for different values of the interaction strength: $\gamma=0.1$ (short-dashed line), $\gamma=0.2$ (dot-dashed line), $\gamma=0.5$ (long-dashed line), $\gamma=1.0$ (dotted line), and $\gamma=3.0$ (full line) compared to that of Eq. (11) of Ref. 32 at $\gamma=1.0$ (thin full line).

$$\hat{Q}_\eta = \int_{-\infty}^{\infty} Q_\eta(x - z_\eta)\hat{\rho}_\eta(x)dx, \quad (81)$$

where kernel $Q_\eta(x) = \int dq\widetilde{Q}_\eta(q)e^{iqx}$ has Fourier transform

$$\widetilde{Q}_\eta(q) = -\frac{i}{q}(e^{i\delta_{q\eta}} - 1). \quad (82)$$

Equation (80) is a key result which has a direct physical interpretation. An electron passing through the interferometer accumulates a phase due to interactions with other electrons. This phase is a collective effect and it is represented at the point where the electron leaves the MZI by the operator $\hat{Q}_\eta$ in Eq. (80). Contributions to the phase from the interactions with particles at a position x from the QPC b have a weight determined by the kernel $Q_\eta(x)$. The form of the kernel is illustrated in Fig. 7 for the case of a charging interaction, studied in Sec. V A. The kernel has a maximum near $x=0$, showing that interactions with nearby electrons are most important, but the phase is influenced by all the electrons which have passed the interferometer, although with contributions which decay with the distance x. The precise form of the kernel depends on the nature of the interaction potential and reflects the full many-body physics of the problem. A similar kernel appears in Eq. (11) of Ref. 32 but with a simpler form because of the approximations employed there. It is shown for comparison in Fig. 7; see discussion in Sec. VI.

Substituting Eq. (80) into Eq. (71) we arrive at

$$\langle \hat{G}_{12}(t)\rangle = e^{i\bar{\Phi}}\langle Fs|[\hat{S}^a(t)]^+\hat{\psi}_1^+(z_1)e^{i\hat{R}}\hat{\psi}_2(z_2)\hat{S}^a(t)|Fs\rangle.$$

Here $\hat{R} = \hat{Q}_1 - \hat{Q}_2$ and $\bar{\Phi} = \varphi_1 - \varphi_2$. The action of $\hat{S}^a(t)^+$ and $\hat{S}^a(t)$ on the operators they enclose is given by Eq. (33). After this transformation the correlator reads

$$\langle \hat{G}_{12}(t) \rangle = e^{i\bar{\Phi}} \frac{1}{L} \sum_{k,q=-\infty}^{\infty} \mathcal{S}_{1\alpha}^{a*} \mathcal{S}_{2\beta}^{a} e^{-ikz_1+iqz_2} \times \langle Fs|[\hat{c}_{k\alpha}^{+} e^{i\hat{\mathcal{R}}} \hat{c}_{q\beta}|Fs \rangle$$

(83)

with summation over repeated indices α, β. Here $\hat{\mathcal{R}} = [\hat{S}^a(t)]^{+} \hat{R} \hat{S}^a(t)$ is the rotated kernel

$$\hat{\mathcal{R}} = \mathcal{S}_{1\alpha}^{a*} \mathcal{S}_{1\beta}^{a} \int_{-\infty}^{\infty} dx Q_1(x-z_1) \hat{\psi}_{\alpha}^{+}(z_1) \hat{\psi}_{\beta}(z_1)$$

$$- \mathcal{S}_{2\alpha}^{a*} \mathcal{S}_{2\beta}^{a} \int_{-\infty}^{\infty} dx Q_2(x-z_2) \hat{\psi}_{\alpha}^{+}(z_2) \hat{\psi}_{\beta}(z_2).$$

(84)

Now evaluation of $\langle \hat{G}_{12}(t) \rangle$ reduces to the calculation of correlators of the form

$$C_{\mu\eta} = \langle Fs|\hat{c}_{\mu}^{+} \exp\left(i \sum_{\alpha\beta} M_{\alpha\beta} \hat{c}_{\alpha}^{+} \hat{c}_{\beta}\right) c_{\eta}|Fs \rangle,$$

(85)

where the indices specify both channel and momentum, and the matrix M is obtained from $\hat{\mathcal{R}}$. One can show (see Appendix C) that $C_{\mu\eta} = D_{\eta\mu}^{-1} \det D$ with D constructed from the matrix elements of $\exp(iM)$ between the single-particle states that are occupied in the Slater determinant $|Fs\rangle$. We calculate $C_{\mu\eta}$ numerically, achieving convergence of the results when keeping up to 10^3 basis states and 400 particles in each channel: further details are given in Appendix D.

V. RESULTS FOR VARIOUS INTERACTION POTENTIALS

In this section we apply our theory to study interferometers with the three types of interaction potential introduced in Sec. III. In the absence of interactions the interferometer at finite bias is specified by four dimensionless parameters: the tunneling probabilities t_a^2 and t_b^2 at the two QPCs; the dimensionless bias $eV\sqrt{d_1 d_2}/2\pi\hbar v_F$; and the ratio of the arm lengths d_2/d_1. The tunneling probability t_b^2 at the second contact QPC affects only the overall scale for visibility of AB oscillations and we set it to $t_b^2 = 1/2$. Interactions in general introduce another parameter, characterizing their strength. Exponential and Coulomb interactions also depend on a further parameter: the interaction range or the short-distance cutoff, respectively.

A. Charging interaction

Consider first the charging interaction, Eq. (13). It is characterized by the single dimensionless coupling constant $\gamma = gd/2\pi\hbar v_F$. Solving Eq. (46) we find

$$f_p(x) = -\left(\frac{2\pi}{qL}\right)^{1/2} \begin{cases} e^{iqx} & x \leq 0 \\ r_p + s_p e^{iqx} & 0 < x < d \\ e^{iqx-i\delta_q} & x \geq d \end{cases}$$

with $q = \omega_p/v_F$. Matching $f_p(x)$ at $x=0$ and $x=d$ gives $s_p = (1+t_p)^{-1}$ and $r_p = t_p s_p$ with $t_p = (g/2\pi i\hbar\omega_p)(e^{i\omega_p d/v_F}-1)$. The phase shift δ_p of plasmons due to the interactions is

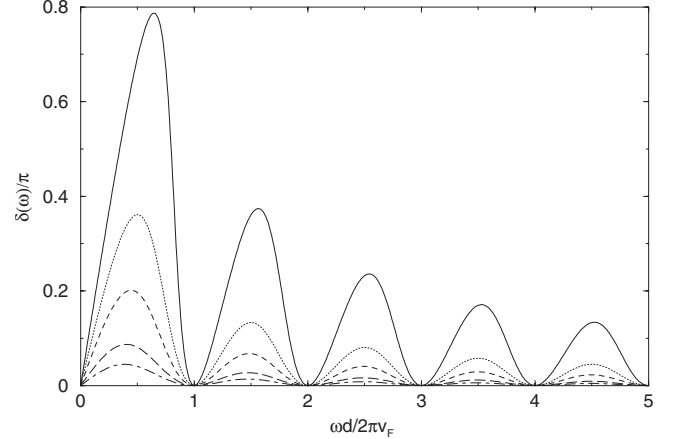$$e^{-i\delta_p} = (1+t_p^*)/(1+t_p).$$

(86)

Similarly, we find

FIG. 8. Frequency dependence of the plasmon phase shift for a charging interaction with strength $\gamma=0.1$ (dot-dashed line), $\gamma=0.2$ (long-dashed line), $\gamma=0.5$ (short-dashed line), $\gamma=1.0$ (dotted line), and $\gamma=3.0$ (full line).

$$\hat{\phi}_0(x) = 2\pi\bar{\gamma}\hat{N}x/L$$

(87)

for $0 \leq x \leq d$, where $\bar{\gamma} = \gamma(1+\gamma)^{-1}$. The contribution $-\frac{1}{2\pi}\partial_x\hat{\phi}_0(x) = -\bar{\gamma}\hat{N}/L$ to the density inside the interferometer represents charge expulsion due to interactions: in the limit of strong interactions the average density inside the interferometer in the stationary regime is pinned at zero, independently of $\hat{N}$.

The plasmon phase shift, as shown in Fig. 8, varies linearly with frequency at low frequency and falls to zero at high frequency. The maximum occurs at a frequency that increases with interaction strength and (for general interactions) depends on the shorter of two lengths: the interaction range and the arm length. For strong interactions, the phase shift at fixed frequency approaches the limiting value $\delta_p = \omega_p d/v_F$. It then exactly cancels the kinetic phase qd. This remarkable cancellation together with the charge expulsion results in behavior independent of arm length when interactions are strong. A similar cancellation was found for a different model in Ref. 30.

We now turn to behavior of the interferometer. We consider first the case $t_a^2 = 1/2$ and $d_1 = d_2$. Results for the visibility of AB fringes as a function of bias voltage and interaction strength are presented in Fig. 9. Without interactions, visibility is independent of bias, having a value fixed by the tunneling probabilities in the QPCs. Interactions generate a dependence of visibility on bias. Visibility at small bias is unaffected by interactions because in this regime there is only one extra electron inside the interferometer at a time but with increasing voltage the visibility follows a sequence of lobes separated by zeros. The width in bias voltage of lobes is inversely proportional to γ for small γ and saturates at a value close to $\pi\hbar v_F/ed$ for $\gamma \gg 1$. The phase of AB fringes is independent of bias inside the lobes and jumps by π at the zeros of visibility. Both features, the lobes in the visibility and the phase slips, match those of experiment by Neder *et al.* (see Figs. 2 and 3 of Ref. 2).
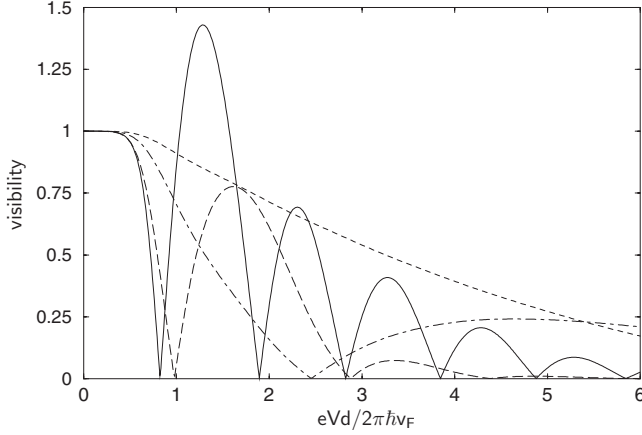
FIG. 9. Visibility as a function of bias voltage for an MZI with charging interactions, and with $d_1 = d_2$ and $t_a^2 = t_b^2 = 1/2$, at interaction strengths: $\gamma = 0.1$ (short-dashed line), $\gamma = 0.2$ (dot-dashed line), $\gamma = 0.5$ (long-dashed line), and $\gamma = 1.0$ (full line). The phase of the AB fringes (not shown) jumps by π at zeros of the visibility.

It is interesting to note that the visibility can become larger than one. This signals a negative value of the differential conductance. Similar behavior has been reported previously.[28]

Results for an interferometer with unequal arm lengths, $d_2/d_1 = 1.2$, are presented in Fig. 10. The gross behavior at intermediate and large interaction strengths is similar to that for an interferometer with equal length arms. The visibility minima for $d_1 \neq d_2$, however, are not exact zeros: they approach zero at large interaction strength but disappear altogether in the opposite limit of weak interactions. There is a corresponding evolution with interaction strength in the dependence of the phase of AB fringes on bias voltage. In the absence of interactions this phase varies linearly with bias for an MZI with different length arms because the Fermi wave vector k_F is linear in bias and the phase difference between particles traversing the two arms is $k_F(d_2 - d_1)$. With increasing interaction strength the phase dependence on bias develops into a series of smooth steps, each of height π. The risers of these steps coincide with minima of the visibility. Strikingly, for the interacting system phase steps at minima of the visibility persist for $d_1 = d_2$ even though in this case phase would be independent of bias without interactions. Between risers the AB phase is almost independent of the ratio d_2/d_1 when interactions are strong because of the cancellation between kinetic and interaction contributions to plasmon phase, as discussed above. The stepwise phase variation we find at large interaction strength also matches experimental observations (see Fig. 2 of Ref. [2]).

Behavior of the visibility is insensitive to the transmission probability t_b^2 at QPC b, apart from the overall scale. Departures from $t_a^2 = 1/2$, however, like unequal arm lengths, eliminate the exact zeros in visibility, leaving only sharp minima. The dependence of visibility on voltage for $t_a^2 = 0.75$ is shown in Fig. 11.

B. Exponential interaction

We next consider the interaction potential of Eq. (15), which decays exponentially with separation. It is character-
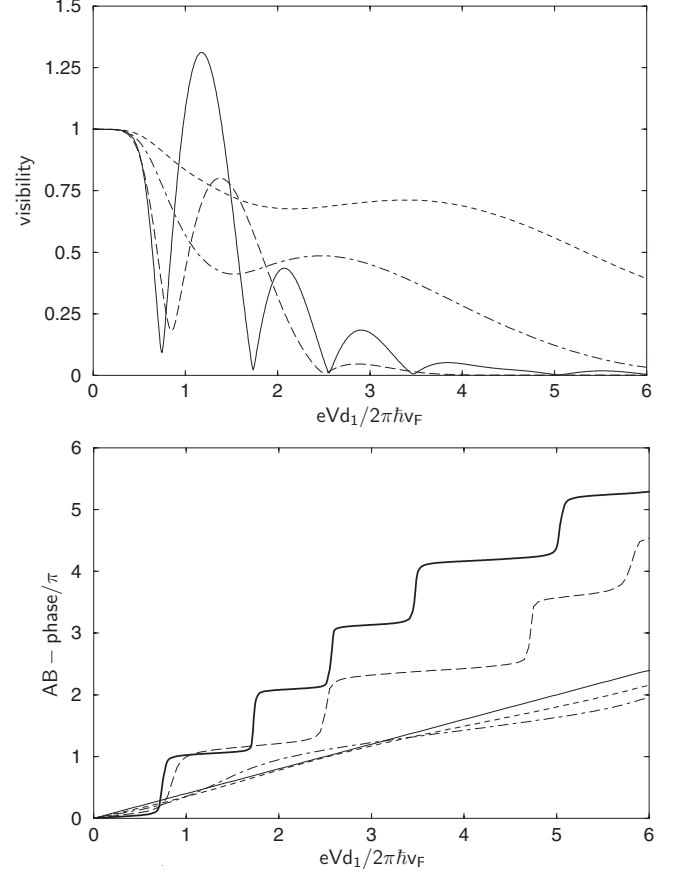

FIG. 10. Visibility (upper panel) and AB phase (lower panel) as a function of bias voltage for an MZI with $d_2/d_1 = 1.2$ and $t_a^2 = t_b^2 = 1/2$ at interaction strengths: $\gamma = 0.1$ (short-dashed line), $\gamma = 0.2$ (dot-dashed line), $\gamma = 0.5$ (long-dashed line), and $\gamma = 1.0$ (full line). The linear dependence of the AB phase in the noninteracting case $\gamma = 0$ is shown on the lower panel (thin full line).

ized by g, the interaction strength, and $1/\alpha$, the range. In this case the Schrödinger equation, Eq. (46), for $0 \leq x \leq d$ has the form

$$-i\omega_p f_p(x) + v_F \partial_x f_p(x) = -\frac{g}{2\pi\hbar} \int_0^d e^{-\alpha|x-y|} \partial_y f_p(y) dy.$$

(88)

Differentiating Eq. (88) twice with respect to x we obtain

$$\partial_{xxx} f_p(x) - i(\omega_p/v_F)[\partial_{xx} f_p(x) - \alpha^2 f_p(x)]$$
$$- (\alpha/d)(2\gamma + \alpha d)\partial_x f_p(x) = 0$$

(89)

with $\gamma = gd/(2\pi\hbar v_F)$ as before. This equation has a solution of the form

$$f_p(x) = \sum_{n=1}^{3} A_n e^{ik_n x},$$

(90)

where the A_n are in general complex coefficients and the wave vectors k_n are obtained by solving the cubic equation

FIG. 12. Frequency dependence of the plasmon phase shift for exponential interactions of strength $\gamma=0.5$ and range: $\alpha d=2$ (dotted line), $\alpha d=1$ (dot-dashed line), $\alpha d=0.5$ (dashed line), and for a charging interaction, $\alpha d=0$ (solid line).

zero at high frequency, are independent of range.

The resulting fringe visibility in an MZI with these interactions is illustrated in Fig. 13. At fixed interaction strength the visibility has zeros at values of the bias voltage which are set by the energy scale $\hbar v_F \alpha$ for interactions with range much shorter than the arm length and by $2\pi\hbar v_F/d$ for interactions with range in the opposite limit.

C. Coulomb interaction

Finally we consider the unscreened Coulomb interaction, Eq. (16), which is characterized by its strength $\gamma_c = g_c/2\pi\hbar v_F$ and the short-distance cutoff a_c. We treat the regime $a_c \ll d$; in the opposite limit it is similar to the charging interaction discussed in Sec. V A. (Coulomb interactions have been studied previously,[28] without our restriction that they act just within the MZI, but only perturbatively in tunneling at QPCs.) To calculate the plasmon phase shifts in this case we solve the Bogoliubov equations [Eq. (65)] numeri-
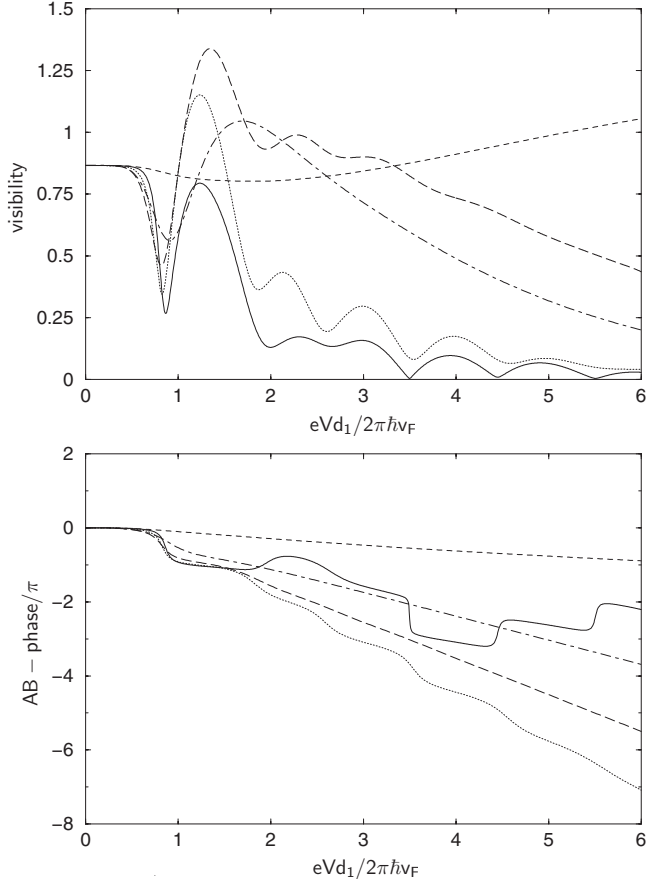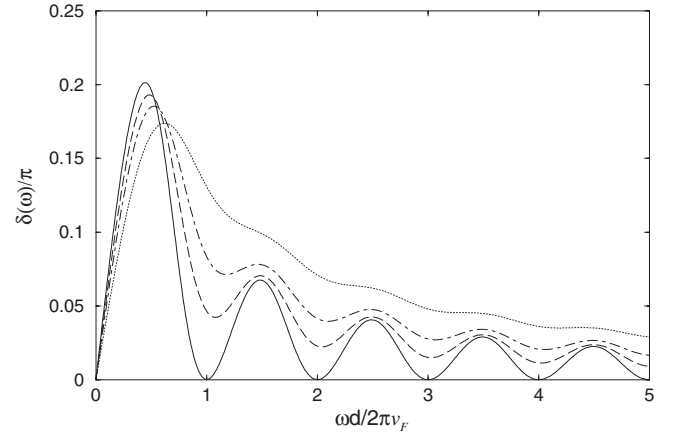

FIG. 11. Visibility (upper panel) and the AB phase (lower panel) as a function of bias voltage for an MZI with $d_2=d_1$, $t_a^2=0.75$, and $t_b^2=1/2$, and charging interactions of strength: $\gamma=0.1$ (short-dashed line), $\gamma=0.5$ (dot-dashed line), $\gamma=1.0$ (long-dashed line), $\gamma=2.0$ (dotted line), and $\gamma=3.0$ (full line).

$$\omega_p = kv_F[1 + \tilde{U}(k)/2\pi\hbar v_F]. \qquad (91)$$

Here $\tilde{U}(k)=2\alpha g/(k^2+\alpha^2)$ is the Fourier transform of the potential in Eq. (15). Substitution of Eq. (90) into Eq. (88) gives two linear equations on A_n and the boundary condition $f_p(0)=1$ yields a third equation. These determine the coefficients A_n and read

$$\sum_{n=1}^{3} A_n = 1, \quad \sum_{n=1}^{3} A_n \frac{k_n e^{ik_n d}}{k_n + i\alpha} = 0,$$

and

$$\sum_{n=1}^{3} A_n \frac{k_n}{k_n - i\alpha} = 0. \qquad (92)$$

Solving Eqs. (90) and (92) numerically we obtain the phase shifts from

$$\delta_p = -\text{Arg}[f_p(d)e^{-i\omega d/v_F}]. \qquad (93)$$

The frequency dependence of this phase shift is shown in Fig. 12 for different values of the interaction range $1/\alpha$ and the interaction strength $\gamma=1$. The main features, of a linear variation at low frequency and a phase shift approaching
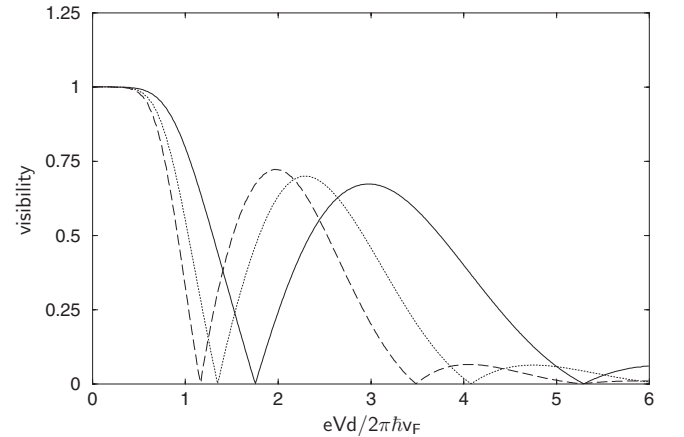

FIG. 13. Visibility as a function of bias voltage for an MZI with exponential interactions [Eq. (15)], with $d_2=d_1$, $t_a^2=t_b^2=1/2$, and $\gamma=0.5$, for interaction ranges: $\alpha d=0.5$ (dashed line), $\alpha d=1$ (dotted line), and $\alpha d=2$ (solid line).
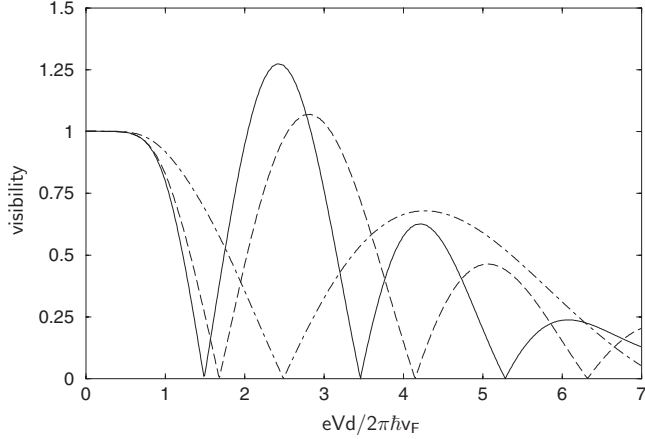
FIG. 14. Visibility as a function of bias voltage for an MZI with unscreened Coulomb interactions [Eq. (16)], taking a short-distance cutoff $a_c = 0.1d_1$, $d_2 = d_1$, $t_a^2 = t_b^2 = 1/2$, and interaction strengths: $\gamma_c = 0.05$ (dot-dashed line), $\gamma_c = 0.1$ (dashed line), and $\gamma_c = 0.15$ (solid line).

cally. Results for the bias dependence of visibility are presented in Fig. 14. The visibility again shows lobes. Their width in bias voltage is inversely proportional to the interaction strength γ_c for weak interactions and is set by the interferometer energy scale $2\pi\hbar v_F/d$ for strong interactions. In summary, while the detailed shape of oscillations in visibility with bias voltage depends on the model used for interactions, the main features are independent of this choice.

VI. DISCUSSION OF THE APPROACH OF NEDER AND GINOSSAR

In a recent paper[32] Neder and Ginossar have presented an approximate treatment of interaction effects in an MZI, using the charging interaction of Eq. (13). They arrive at a result similar in form to the exact one given above in Eqs. (80) and (81) but with a different kernel $Q(x)$: see the comparison in Fig. 7. Making further simplifications in the course of a numerical evaluation, they obtain nodes in the dependence of visibility on bias voltage. We discuss their approach in this section (we note that various choices of kernel and of approximations schemes in this type of numerical evaluation have also been discussed in Ref. 31). We show that their central approximation is equivalent to neglect of the chiral anomaly in the Tomonaga-Luttinger model, and explain physically what this entails. We also examine how far the differences between results for visibility in Ref. 32 and those in the present paper are due to this central approximation, and how far they stem from simplifications of the numerical evaluation made in Ref. 32. To do this we make a numerically exact calculation of the fringe visibility using the kernel of Ref. 32 and compare the outcome with our own results.

A. Single edge with translationally invariant interactions

The approach under discussion starts from the Heisenberg equation of motion for an operator $\hat{A}_H(t)$. Consider first a

single edge channel without QPCs. In this case the equation of motion is

$$i\hbar\partial_t \hat{A}_H(t) = [\hat{A}_H(t), H_0] \tag{94}$$

with initial condition $\hat{A}_H(0) = \hat{A}$, where $\hat{A}$ is the operator in the Schrödinger representation. In the absence of interactions Eq. (94) for the field operator has the solution

$$\hat{\psi}_H^+(d,t) = \hat{\psi}_H^+(\varepsilon, t - d_\eta/v_F). \tag{95}$$

Next, include translationally invariant interactions $U(x, x') = U(x - x')$ with $U(0) = 0$ to avoid self-interactions. The equation of motion is

$$i\hbar(\partial_t + v_F\partial_x)\hat{\psi}_H^+(x,t) = -\hat{\psi}_H^+(x,t)\int_{-\infty}^{\infty} U(x - x')\hat{\rho}_H(x',t)dx'. \tag{96}$$

It apparently has the solution

$$\hat{\psi}_H^+(x,t) = e^{i\hat{\theta}_H(x,t)}\hat{\psi}_H^+(x - v_F t, 0), \tag{97}$$

where the phase operator $\hat{\theta}_H(x,t)$ is given by

$$\hat{\theta}_H(x,t) = \frac{t}{\hbar}\int_{-\infty}^{\infty} U(x')\hat{\rho}(x - v_F t + x', 0)dx'. \tag{98}$$

This calculation is essentially a version in the Heisenberg picture of the solution of the Tomonaga-Luttinger model by Luttinger,[37] who used a canonical transformation to diagonalize the Hamiltonian. It is exact provided the number of particles in the system is finite. The difficulty, of course, is that for finite particle number a model with linear dispersion has no ground state and so one wants to introduce a filled Fermi sea. Unfortunately, as shown by Leib and Mattis,[38] the calculation is then no longer exact because density operators which commute when particle number is finite no longer do so in the presence of the Fermi sea.

To illustrate the difference in physical behavior between a system with a finite number of particles and one with a Fermi sea, it is useful to consider the time evolution of an initial state in which single-particle orbitals are all occupied for wave vectors k in the range $0 \le k \le k_F$ and others are all empty. We denote this state by $|k_F\rangle$ and compare its evolution with that of the state with a Fermi sea, in which *all* orbitals with $k \le k_F$ are occupied. The latter is an exact eigenstate of $\hat{H}_0$ for arbitrary choice of interaction and so has trivial time evolution. By contrast, $|k_F\rangle$ is not an eigenstate in the presence of interactions. To be specific, we calculate the time dependence of the particle number $\hat{n}(Q) = \hat{c}_Q^+\hat{c}_Q$ in an orbital with wave vector Q. Within a short-time expansion we have

$$\langle\hat{n}(Q,t)\rangle = \langle\hat{n}(Q)\rangle + it\langle[\hat{H}_0, \hat{n}_Q]\rangle - \frac{t^2}{2}\langle[\hat{H}_0, [\hat{H}_0, \hat{n}_Q]]\rangle\ldots$$

$$\tag{99}$$

For the state $|k_F\rangle$ the average $\langle[\hat{H}_0, \hat{n}(Q)]\rangle = 0$. The second-order term is conveniently expressed in terms of

$$\tilde{U}(q) = \int_{-\infty}^{\infty} dx U(x) e^{iqx} \tag{100}$$

the Fourier transform of the interaction potential. Taking k_F^{-1} to be much smaller than the interaction range, and writing $Q = k_F + P$ with $P > 0$, we find

$$\langle \hat{n}(Q,t) \rangle = t^2 \langle \hat{H}_0 \hat{n}(Q) \hat{H}_0 \rangle + \cdots = \frac{t^2}{8\pi^2} \int_P^{\infty} dq q |\tilde{U}(q)|^2 + \mathcal{O}(t^3).$$

Similarly, for $-k_F \ll P < 0$ we obtain

$$\langle \hat{n}(Q,t) \rangle = 1 - \frac{t^2}{8\pi^2} \int_{-P}^{\infty} dq q |\tilde{U}(q)|^2 + \mathcal{O}(t^3). \tag{101}$$

This shows that interactions scatter particles from the orbitals they occupy initially in $|k_F\rangle$ to others of larger and smaller energy. The pair of particles involved in a typical scattering event has one initial wave vector just less than k_F and the other just larger than zero. One particle is scattered to a state with wave vector $k > k_F$ and the other to a state with negative wave vector. The rate for this process remains finite even when k_F is large but in the presence of a Fermi sea these scattering processes are blocked by Pauli exclusion.

B. Interactions confined to a finite region

To demonstrate that no other approximations are involved in the derivation of the kernel of Ref. 32, we next set out a calculation equivalent to the one leading to Eq. (97), but for interactions that operate only in the finite region $0 < x < d$ and are translationally invariant within this region, so that

$$\hat{\mathcal{H}}_{int} = \frac{1}{2} \int_0^d \int_0^d U(x - x') \hat{\rho}(x) \hat{\rho}(x') dx dx'. \tag{102}$$

Then the equation of motion for $\hat{\psi}^+(x,t)$ can be solved by integrating forward in time separately in each of three regions and matching at boundaries. For $x < 0$ we have

$$\hat{\psi}^+(x,t) = \hat{\psi}^+(x - v_F t, 0). \tag{103}$$

Within the approximation under discussion, for $0 < x < d$

$$\hat{\psi}_H^+(x,t) = e^{i\hat{\theta}_H(x,t)} \hat{\psi}_H^+(x - v_F t, 0), \tag{104}$$

where $\hat{\theta}_H(x,t)$ satisfies the equation

$$(\partial_t + v_F \partial_x) \hat{\theta}_H(x,t) = \frac{1}{\hbar} \int_0^d U(x - x') \hat{\rho}_H(x',t) dx' \tag{105}$$

with the boundary condition $\hat{\theta}(0,t) = 0$. This has the solution

$$\hat{\theta}_H(x,t) = \frac{1}{\hbar v_F} \left\{ \int_{-v_F t}^{x - v_F t} (x' + v_F t) + x \int_{x - v_F t}^{d - v_F t} \right.$$
$$\left. + \int_{d - v_F t}^{d + x - v_F t} (d + \tilde{x}) \right\} \times U(\tilde{x}) \hat{\rho}_H(x', 0) dx' \tag{106}$$

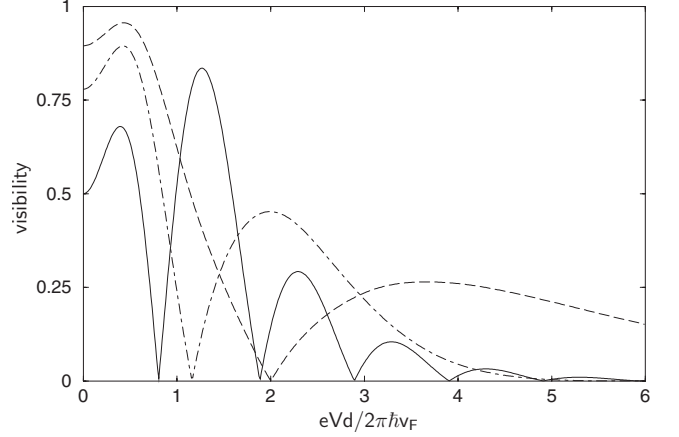in which $\tilde{x} = x - v_F t - x'$.

FIG. 15. Visibility as a function of bias voltage for an MZI with charging interactions, calculated using the kernel of Eq. (11) of Ref. 32, with $d_1 = d_2 = 1$ and $t_a^2 = t_b^2 = 1/2$, for interaction strengths: $\gamma = 0.1$ (dashed line), $\gamma = 0.2$ (dot-dashed line), and $\gamma = 0.5$ (solid line).

In particular, for $x = d$ we have

$$\hat{\theta}_H(d,t) = \frac{1}{\hbar v_F} \int_0^d x' U(d - x') \hat{\rho}_H(x',t) dy$$
$$+ \frac{1}{\hbar v_F} \int_d^{2d} (2d - x') U(d - x') \hat{\rho}_H(x',t) dx'. \tag{107}$$

In the region $x > d$ we can use results from $0 < x < d$ as a boundary condition to obtain

$$\hat{\psi}_H^+(x,t) = e^{i\hat{\theta}_H(d,t)} \hat{\psi}_H^+(x - v_F t, 0). \tag{108}$$

For the charging interaction, Eq. (13), this gives an expression for the kernel $Q(x)$ appearing in Eq. (81) which is equivalent to Eq. (11) of Ref. 32.

C. Interferometer with internal interactions

For an interferometer with only internal interactions, the foregoing discussion can be combined with the approach described in Secs. IV A–IV E. In particular, making use of Eq. (108) in place of Eq. (82), one arrives at alternative results for visibility. We have evaluated these without further approximation for charging interactions. They are displayed in Fig. 15. In this approximation the visibility as a function of bias shows a lobe pattern similar to that given by our exact solution (Fig. 9) but some significant differences are apparent. In particular, within the approximate treatment visibility at small bias is reduced from its value in the noninteracting system and more so as interaction strength is increased. This loss of coherence mirrors the scattering described by Eq. (101). It is not a feature of the exact treatment for a system with a Fermi sea: in that case at small bias extra electrons are dilute and pass independently through the interferometer.

VII. PERTURBATION THEORY IN INTERACTIONS

The approach we have used to obtain exact results can be applied only to models in which interactions act solely

TABLE I. Amplitudes of the scattering state $\varphi_{q1}(x,\kappa)$.

κ	$x<0$	$0<x<d_\kappa$	$d_\kappa<x$
1	1	r_a	$r_a r_b - t_a t_b e^{i(q[d_2-d_1]+\beta-\alpha)}$
2	0	$-it_a e^{-i\alpha}$	$-it_a r_b e^{-i\alpha} - i r_a t_b e^{i(q[d_1-d_2]-\beta)}$

within the MZI. In order to gain some understanding of the consequences of more general interactions, it is useful to formulate perturbation theory in powers of interaction strength. We outline such a calculation in this section. Since details are quite messy (around forty separate terms appear at first order in interaction strength), we limit ourselves to sketching how a new physical effect—a second harmonic in the variation in differential conductance with AB flux—appears when there are interactions between the interior and exterior of the MZI. This expansion in powers of interaction strength, which can be applied for arbitrary values of the tunneling amplitude at QPCs, is complementary to the perturbation theory in tunneling strength, developed for arbitrary interaction strength in Ref. 28.

We separate the Hamiltonian, Eq. (7), into the single-particle contribution $\hat{H}_1 = \hat{\mathcal{H}}_{kin} + \hat{\mathcal{H}}_{tun}$ and the interaction term $\hat{\mathcal{H}}_{int}$, and start from a single-particle basis of scattering states of $\hat{H}_1$. These states are labeled by energy $\hbar v_F q$ and by the channel η (denoted 1 and 2 in Fig. 6) from which particles are incident on the MZI. They have amplitude $e^{iqx}\varphi_{q\eta}(x,\kappa)$ at point x in channel κ. Thus, for example, $\varphi_{q1}(x,\kappa)$ takes the form given in Table I.

We consider an initial many-particle wave function $|\Psi_0\rangle$ in which scattering states are occupied up to Fermi wave vectors p_1 and p_2, respectively, in the two incident channels, representing a bias voltage $V = \hbar v_F(p_1 - p_2)/e$. Using the interaction representation $\hat{A}(t) = e^{i\hat{H}_1 t/\hbar}\hat{A}e^{-i\hat{H}_1 t/\hbar}$ based on $\hat{H}_1$ (different, of course, from that employed in Sec. IV), we evolve the initial state forward in time from $t=-\infty$ to $t=0$. The current at zeroth and first order in $\hat{\mathcal{H}}_{int}$ is

$$\langle \hat{I}(t)\rangle_{t=0} = \langle\Psi_0|\hat{I}(0)|\Psi_0\rangle + \frac{i}{\hbar}\int_{-\infty}^{0}\langle\Psi_0|[\hat{\mathcal{H}}_{int}(\tau),\hat{I}(0)]|\Psi_0\rangle d\tau. \tag{109}$$

To evaluate the interaction term in this expression we take matrix elements in the basis of single-particle scattering states, denoting for brevity the pair of labels q_a, κ_a by a. For an interaction $U(x,x')$ that does not couple channels we write

$$\bar{U}_{abcd} = \frac{1}{2}\int\int dx dx' U(x,x')e^{i[(q_d-q_a)x+(q_c-q_b)x']}$$

$$\times \sum_\kappa \varphi^*_{q_a\kappa}(x)\varphi^*_{q_b\kappa}(x')\varphi_{q_c\kappa}(x')\varphi_{q_d\kappa}(x) \tag{110}$$

and define the antisymmetrized combination $U_{abbd} = \frac{1}{2}(\bar{U}_{abbd} - \bar{U}_{abdb})$. We evaluate matrix elements I_{ab} of the current operator by considering in the first instance a tunneling contact

of finite width w, then taking the limit $w\to 0$, as in Sec. IV A. For example,

$$I_{k1q1} = ev_F(t_a^2 + r_a^2 t_b^2 e^{id_1(q-k)} - t_a^2 t_b^2 e^{id_2(q-k)}$$

$$+ t_a r_a t_b r_b[e^{i(\alpha-\beta+qd_1-kd_2)} + e^{i(\beta-\alpha+qd_2-kd_1)}]).$$

With this notation, and denoting by n_a the average occupation of the state a, the first-order term from Eq. (109) has the form

$$\frac{i}{2\pi^3\hbar}\int_{-\infty}^{0}d\tau\int_{-\infty}^{\infty}dk_a\int_{-\infty}^{\infty}dk_b\int_{-\infty}^{\infty}dk_c$$

$$\times U_{abbc}I_{ca}n_b(n_a - n_c)e^{iv_F(k_a-k_c)\tau}.$$

Evaluating the integrals on τ, k_a, k_b, and k_c we obtain an expression in which only integration on x and x' from Eq. (110) remains. Because the factors $\varphi_{q\eta}(x,\kappa)$ take different forms in each of the regions I, II, and III, defined in Fig. 6, these final integrals naturally separate into distinct contributions according to the possible locations of each of two interacting particles.

As an illustration of this general approach we consider the contribution to current arising at first order from the interaction between a particle in region II and one in region III. This is made up of an exchange term δI_F^{23} and a Hartree term δI_H^{23}. To write expressions for these in a concise form we limit ourselves to the case $d_1 = d_2 \equiv d$ and define the constant $\mathcal{T}_{ab} = t_a t_b r_a r_b$. Then

$$\delta I_F^{23} = -\frac{8e\mathcal{T}_{ab}^2}{\pi\hbar}\sin 2\Phi$$

$$\times \int_0^d dx \int_d^\infty dx' U(x,x')\frac{\sin^2[(p_1-p_2)(x-x')/2]}{(x-x')^2}$$

and

$$\delta I_H^{23} = \frac{2e\mathcal{T}_{ab}^2}{\pi\hbar}(p_1-p_2)^2\sin 2\Phi \times \int_0^d dx \int_d^\infty dx' U(x,x').$$

As advertised, both terms involve the second harmonic $\sin 2\Phi$ of the AB phase Φ. They display the antisymmetry expected for the current under reversal of both V and Φ. A second harmonic is also produced by the interactions between the electrons in the regions I and III which we do not present here. By contrast, a similar perturbative treatment of interactions between electrons in region II generates only zeroth and first harmonics of Φ, as expected from the results presented in Sec. IV.

VIII. DISCUSSION

In summary, we have argued that electron interactions are the origin of the experimentally observed dependence of visibility of AB oscillations on bias voltage in electronic MZIs. This is illustrated most simply by calculations of two-particle interference effects, described in Sec. II, and demonstrated in detail by exact results for the many-body system, presented in Sec. V. Our calculations rely on a simplified form for interactions but we believe our choice is quite reasonable.

Our central approximation is to neglect interactions between an electron inside the MZI and one outside. In practice, such interactions will anyway be screened by the metal gates that define the QPCs. We also neglect interactions between a pair of electrons that are both outside the MZI. This is unimportant: before electrons reach the MZI, such interactions do not cause scattering because of Fermi statistics, while after electrons pass through the MZI, these interactions cannot affect the current. We have given results for three forms of interaction within the MZI, finding their main features to be independent of details of the model. These features include a series of lobes of decreasing amplitude in AB fringe visibility as a function of bias, with jumps by π in the phase of AB oscillations near minima in visibility.

The width in bias voltage of the central visibility lobe defines an energy scale. For our model of charging interactions this scale is of order g at large γ. Taking $v_F = 2.5 \times 10^4$ ms^{-1}, $d = 10$ μm, and the permittivity $\epsilon = 12.5$ of GaAs, we estimate from the capacitance of an edge channel $g \sim 10$ μeV. This is similar to the experimentally observed value of about 14 μeV, given in Ref. 2.

We close by comparing the results we have presented with those from other approaches. As a first step, we note that, while the existence of multiple side lobes in the visibility of AB oscillations as a function of bias voltage cannot be accounted for by a simple treatment of dephasing, a single-side lobe can emerge from a simple, phenomenological treatment. To see this, consider the dependence of current $I(V, \Phi)$ on bias V and AB flux Φ. Assuming that there is a just one harmonic in AB oscillations, we have

$$I(V, \Phi) = I_0(V) + I_1(V)\cos[\Phi + \theta(V)]. \quad (111)$$

With this notation, the visibility is

$$\mathcal{V} = \frac{[[\partial_V I_1(V)]^2 + [I_1(V)\partial_V \theta(V)]^2]^{1/2}}{|\partial_V I_0(V)|}. \quad (112)$$

It is reasonable to expect quite generally that $I_1(V)$ increases with V for small V, has a single maximum, and decreases toward zero at large V, so that $\partial_V I_1(V)$ has a single zero for $0 \leq V < \infty$. If in addition the phase $\theta(V)$ of AB oscillations is independent of V (and only in this case), the existence of a single-side lobe in visibility follows.

The theoretical difficulty, then, is to understand the observation of multiple-side lobes. Calculations to date that generate such behavior can be divided into three categories. One of these[29] involves a plasmon resonance between one arm of the MZI and a counterpropagating edge state at the boundary of the Hall bar. Such a coupling of the MZI to another edge state is not an essential part of the interferometer design and in this sense the mechanism is not an intrinsic one. For that reason, it seems unlikely to provide the explanation for observations in many different samples of varying designs. The most important comparison is therefore between a second category of explanation,[30] which is based on coupling between the two channels existing at each edge for filling factor $\nu = 2$, and the third category, which is formed by the cal-

culations that we have presented, together with earlier approximate discussions[32,33] of similar physics, and has been worked out for a system at $\nu = 1$.

According to the approach of Ref. 30, multiple-side lobes should be found only at $\nu = 2$, which seems indeed to be the case experimentally. Some important discrepancies between this theory and experiment remain, however. One is that, within the approach of Ref. 30, the shape of the envelope of the lobe pattern is controlled by the difference in interferometer arm lengths: in particular, for an interferometer with arms of equal length, visibility does not fall to zero at large bias. This is in conflict with observations. It requires one to assume[30] that two separate physical processes are involved: the process included in the theory, which leads to multiple zeros in visibility at $\nu = 2$, and another one, omitted from the theory (such as dispersion of the edge modes), which controls decay of the envelope. Moreover, if this theory is adopted at $\nu = 2$, the existence of a single-side lobe at $\nu = 1$ must be attributed to a separate dephasing mechanism, following Eq. (112). In experiment, there appears to be a common voltage scale determining all aspects: the zeros in visibility at $\nu = 2$, the envelope of the lobe pattern at either filling factor, and the position of the visibility zero at $\nu = 1$. It would be a surprising coincidence if two separate mechanisms were both to involve the same scale. An explanation of multiple-side lobes in visibility based exclusively on dispersionless slow and fast edge modes at $\nu = 2$ therefore seems problematic. By contrast, the calculations we have presented generate zeros of visibility and an overall decaying envelope for visibility from a single mechanism. Depending on interaction strength we find either multiple-side lobes or only a single prominent side lobe. The mechanism is essentially plasmon dispersion. It is likely that a full understanding of experiments will require a combination of both aspects—dispersion and the existence of two modes at $\nu = 2$. It is however, an important point of principle, demonstrated by the calculations we have described, that multiple-side lobes are not an exclusive consequence of coupling between a slow and a fast mode at $\nu = 2$.

A definite qualitative feature of our results is that exact zeros of fringe visibility at certain values of bias voltage appear only for an interferometer with equal length arms, in which the transmission probability at the first QPC is tuned precisely to the value one half. Changes in transmission probability and (though to a much lesser extent, if interactions are strong) arm length from these values convert exact zeros to finite minima in visibility. Such sensitivity to transmission probability has not been reported experimentally. The reason it appears in our theory can be understood starting from Eq. (112): exact zeros of visibility can occur only if the phase $\theta(V)$ of AB oscillations is independent of bias V. A phase independent of bias is ensured by symmetry for an interferometer with $L_1 = L_2$ and $t_a^2 = 1/2$. For other parameter choices, our model, in which there are no interactions between electrons on opposite interferometer arms, yields a bias-dependent $\theta(V)$, essentially because that Hartree potentials for electrons on each arm vary differently with V. For this reason, it would be interesting to generalize our treatment to systems with interactions between edges as well as within each edge. We expect that such interactions would

reduce or eliminate the dependence of $\theta(V)$ on V, giving near or exact zeros of visibility even for $t_a^2 \neq 1/2$ or $L_1 \neq L_2$, in accord with experiment. Other possible generalizations include calculation of finite temperature effects and of noise power.

APPENDIX A: CALCULATION OF THE COMMUTATION RELATIONS

We wish to show that the commutators $[\hat{\mathcal{H}}_{tun}^a(t_1), \hat{\mathcal{H}}_{tun}^b(t_2)]$ and $[\hat{G}_{12}(t_1), \hat{\mathcal{H}}_{tun}^b(t_2)]$ appearing in Sec. IV B are zero for $t_1 \geq t_2$. As a first step we obtain commutation relations for the fermion fields appearing in Eq. (80) of Sec. IV F. To keep notation concise, we define

$$\hat{\Psi}_\eta(z_\eta) \equiv \hat{\psi}_\eta(d_\eta, t) = e^{-i\int_{-\infty}^{\infty} Q_\eta(x - z_\eta)\hat{\rho}_\eta(x)dx}\hat{\psi}_\eta(z_\eta),$$

where $z_\eta = d_\eta - v_F t$. The kernel $Q_\eta(z)$ is nonzero only for $z > -d_\eta$. This follows from causality (with interactions occurring only inside the interferometer, the phase of an electron at QPC b cannot be influenced by electrons that have yet to enter the MZI) and can be demonstrated explicitly for the case of charging interactions, using the analytic structure of the phase shifts, Eq. (86). We have

$$\{\hat{\psi}_\eta(x), \hat{\Psi}_{\eta'}(x')\} = 0, \quad \{\hat{\psi}_\eta(x), \hat{\Psi}_{\eta'}^+(x')\} = 0 \quad \text{(A1)}$$

for any η, η' and $x' - x \geq d_\eta$. From this we find

$[\hat{\mathcal{H}}_{tun}^a(t_1), \hat{H}_{tun}^b(t_2)]$

$= [v_a e^{i\alpha}\hat{\psi}_1^+(-v_F t_1)\hat{\psi}_2(-v_F t_1)$

$+ \text{H.c.}, v_b e^{i\beta}\hat{\Psi}_1^+(d_1 - v_F t_2)\hat{\Psi}_2(d_2 - v_F t_2) + \text{H.c.}] = 0$

for $t_1 \geq t_2$.

We also require the anticommutators of $\hat{\Psi}_\eta(x)$ with itself and with $\hat{\Psi}_\eta^+(x)$. These are straightforward to obtain starting from the bosonized form for the fermion operators. However, it is instructive also to derive them directly from the representation in Eq. (80), as follows. We have

$$\hat{\Psi}_\eta(x)\hat{\Psi}_{\eta'}(x') = -\hat{\Psi}_{\eta'}(x')\hat{\Psi}_\eta(x)$$
$$\times e^{-[\hat{Q}_\eta, \hat{Q}_{\eta'}]} e^{i[Q_\eta(x'-x) - Q_\eta(x-x')]\delta_{\eta\eta'}},$$

where

$$[\hat{Q}_\eta, \hat{Q}_{\eta'}] \equiv \int_{-\infty}^{\infty} Q_\eta(z - x)Q_{\eta'}(z' - x')$$
$$\times [\hat{\rho}_\eta(z), \hat{\rho}_{\eta'}(z')]dzdz'.$$

Because of the presence of the filled Fermi sea, the density operators do not commute.[35] Instead

$$[\hat{\rho}_\eta(z), \hat{\rho}_{\eta'}(y)] = -\frac{i}{2\pi}\partial_z\delta(z - y)\delta_{\eta\eta'}.$$

From this

$$[\hat{Q}_\eta, \hat{Q}_{\eta'}] = \frac{i}{2\pi}\int_{-\infty}^{\infty} dy Q(y - x')\partial_y Q(y - x).$$

We now prove that

$$Q(x' - x) - Q(x - x') = \frac{1}{2\pi}\int_{-\infty}^{+\infty} dy Q(y - x')\partial_y Q(y - x).$$

Introducing the Fourier transform of the kernel we have

$$Q(x' - x) - Q(x - x') = \int dq\widetilde{Q}(q)[e^{iq(x'-x)} - e^{iq(x-x')}]$$

and

$$\frac{1}{2\pi}\int_{-\infty}^{+\infty} dy Q(y - x')\partial_y Q(y - x) = i\int dqq\widetilde{Q}(q)\widetilde{Q}(-q)e^{iq(x'-x)}.$$

Thus we wish to show

$$\widetilde{Q}(q) - \widetilde{Q}(-q) = iq\widetilde{Q}(q)\widetilde{Q}(-q).$$

It is easy to check that this is the case, using the explicit form

$$\widetilde{Q}(q) = 2\pi\gamma dj_0^2(qd/2)[1 + \gamma e^{-iqd/2}j_0(qd/2)]^{-1}$$

for the kernel in the case of a charging interaction, where $j_0(x) = (\sin x)/x$. This gives

$$\{\hat{\Psi}_\eta(x), \hat{\Psi}_{\eta'}(x')\} = 0,$$

$$\{\hat{\Psi}_\eta(x), \hat{\Psi}_{\eta'}^+(x')\} = \delta_{\eta\eta'}\delta(x - x').$$

It follows directly that $[\hat{G}_{12}(t), \hat{\mathcal{H}}_{tun}^b(t')] = 0$ for $t \geq t'$.

APPENDIX B: CALCULATION OF THE S–MATRIX

We require an explicit form for the unitary transformation of fermion operators generated by

$$\hat{S}^a(t) = T\exp\left\{-\frac{i}{\hbar}\int_0^t \hat{\mathcal{H}}_{tun}^a(\tau)d\tau\right\}. \quad \text{(B1)}$$

The fermion operators appearing in $\hat{\mathcal{H}}_{tun}^a$ commute with $\hat{\mathcal{H}}_{int}$ because their position coordinates are before the interacting region. For this reason the interaction representation of $\hat{\mathcal{H}}_{tun}^a(\tau)$ has the simple form

$$\hat{\mathcal{H}}_{tun}^a(\tau) = v_a e^{i\alpha}\hat{\psi}_1^+(-v_F\tau)\psi_2(-v_F\tau) + \text{H.c.}$$

The Schrödinger operators $\hat{\psi}_\eta(-v_F\tau)$ anticommute at different values of their argument. As a consequence

$$[\hat{\mathcal{H}}_{tun}^a(\tau), \hat{\mathcal{H}}_{tun}^a(\tau')] = 0$$

for any τ, τ' and the time ordering in Eq. (B1) can be omitted.

Defining

$$\tilde{\tilde{\psi}}_\eta(x,t) = \hat{S}^{a+}(t)\hat{\psi}_\eta(x)\hat{S}^a(t) \tag{B2}$$

and using a Baker-Hausdorff formula

$$e^{-B}Ae^{B} = \sum_{n=0}^{\infty}\frac{1}{n!}[A,B]_n = A + [A,B] + \frac{1}{2!}[[A,B],B] + \cdots$$

we obtain

$$\tilde{\tilde{\psi}}_\eta(x,t) = \begin{cases} \displaystyle\sum_{\mu=1,2}\mathcal{S}^a_{\eta\mu}\hat{\psi}_\mu(x) & -v_F t \le x < +0 \\[2mm] \hat{\psi}_\eta(x) & \text{otherwise}, \end{cases} \tag{B3}$$

where

$$\mathcal{S}^a = \begin{pmatrix} r_a & -it_a e^{i\alpha} \\ -it_a e^{-i\alpha} & r_a \end{pmatrix}.$$

APPENDIX C: MATRIX ELEMENTS OF THE EXPONENTIAL OPERATOR

Here we present a derivation of the equation which we use to evaluate matrix elements of the form

$$C_{kl} \equiv \langle\alpha|\hat{c}_k^+ e^{i\sum_{ij} M_{ij}\hat{c}_i^+\hat{c}_j}\hat{c}_l|\beta\rangle, \tag{C1}$$

where the fermionic operators $\hat{c}_i$ obey usual anticommutation relations $\{\hat{c}_i,\hat{c}_j^+\}=\delta_{ij}$ and $\{\hat{c}_i,\hat{c}_j\}=0$. The matrix M_{ij} is Hermitian and so the exponential

$$\hat{U} = e^{i\sum_{ij} M_{ij}\hat{c}_i^+\hat{c}_j} \tag{C2}$$

is a unitary operator. The matrix elements C_{kl} are calculated with respect to the states

$$|\alpha\rangle = |m_1, m_2, \ldots, m_N\rangle, \tag{C3}$$

$$|\beta\rangle = |n_1, n_2, \ldots, n_N\rangle \tag{C4}$$

with fermions occupying single-particle levels enumerated as $m_1 < m_2, \ldots, < m_N$ and $n_1 < n_2, \ldots, < n_N$ correspondingly, here N is a total number of electrons. We can write these states as a product of creation operators acting on vacuum

$$|\alpha\rangle = \hat{c}_{m_N}^+\hat{c}_{m_{N-1}}^+, \ldots, \hat{c}_{m_1}^+|vac\rangle, \tag{C5}$$

$$|\beta\rangle = \hat{c}_{n_N}^+\hat{c}_{n_{N-1}}^+, \ldots, \hat{c}_{n_1}^+|vac\rangle. \tag{C6}$$

The matrix elements in Eq. (C1) can be written as

$$C_{kl} = \langle vac|\hat{c}_{m_1}\hat{c}_{m_2}, \ldots, \hat{c}_{m_N} \times \hat{c}_k^+\hat{U}\hat{c}_l\hat{c}_{n_N}^+\hat{c}_{n_{N-1}}^+ \ldots \hat{c}_{n_1}^+|vac\rangle \tag{C7}$$

or after commuting the operator $\hat{c}_k^+$ to the left and $\hat{c}_l$ to the right we obtain

$$C_{kl} = (-1)^{p+q}\langle vac|\hat{c}_{m_1}\hat{c}_{m_2}, \ldots, \hat{c}_{m_{p-1}}\hat{c}_{m_{p+1}}, \ldots, \hat{c}_{m_N}$$
$$\times \hat{U}\hat{c}_{n_N}^+\hat{c}_{n_{N-1}}^+, \ldots, \hat{c}_{n_{q+1}}^+\hat{c}_{n_{q-1}}^+, \ldots, \hat{c}_{n_1}^+|vac\rangle, \tag{C8}$$

where p and q are defined such that $k=m_p$ and $l=n_q$. Now

using the unitarity of the $\hat{U}$ matrix we can rewrite it as

$$C_{kl} = (-1)^{p+q}\langle vac|\hat{c}_{m_1}\hat{c}_{m_2}, \ldots, \hat{c}_{m_{p-1}}\hat{c}_{m_{p+1}}, \ldots, \hat{c}_{m_N}$$
$$\times \hat{U}\hat{c}_{n_N}^+\hat{U}^+\hat{U}\hat{c}_{n_{N-1}}^+\hat{U}^+, \ldots, \hat{U}\hat{c}_{n_{q+1}}^+\hat{U}^+\hat{U}\hat{c}_{n_{q-1}}^+\hat{U}^+, \ldots,$$
$$\times \hat{U}\hat{c}_{n_1}^+\hat{U}^+\hat{U}|vac\rangle. \tag{C9}$$

Using the fact that $\hat{U}|vac\rangle=|vac\rangle$ we arrive at the equation

$$C_{kl} = (-1)^{p+q}\langle vac|\hat{c}_{m_1}\hat{c}_{m_2}, \ldots, \hat{c}_{m_{p-1}}\hat{c}_{m_{p+1}}, \ldots, \hat{c}_{m_N}$$
$$\times \tilde{c}_{n_N}^+\tilde{c}_{n_{N-1}}^+, \ldots, \tilde{c}_{n_{q+1}}^+\tilde{c}_{n_{q-1}}^+, \ldots, \tilde{c}_{n_1}^+|vac\rangle, \tag{C10}$$

where we defined $\tilde{c}_i^+ = \hat{U}\hat{c}_i^+\hat{U}^+$. Applying the Baker-Hausdorff identity we obtain

$$\tilde{c}_i^+ = \sum_{n=0}^{\infty}\frac{i^n}{n!}M_{ii_1}^T M_{i_1 i_2}^T, \ldots, M_{i_{n-1}i_n}^T\hat{c}_{i_n}^+ = \sum_{j=0}^{\infty}U_{ij}^T\hat{c}_j^+, \tag{C11}$$

where matrix U is defined as

$$U = \exp[iM]. \tag{C12}$$

Substituting Eq. (C11) into Eq. (C10) gives an equation for the matrix elements

$$A_{kl} = D_{lk}^{-1}\det D, \tag{C13}$$

where matrix D is formed from the matrix elements U_{ij} with indices i and j spanning the occupied states $m_1, m_2, \ldots, m_N$ and $n_1, n_2, \ldots, n_N$ correspondingly.

APPENDIX D: NUMERICAL EVALUATION OF THE CORRELATORS

In this appendix we provide details of the numerical procedure, outlined in Sec. IV F, which we use at the final stage of our calculations to evaluate the correlation functions from Eq. (83). We consider a system of length L with periodic boundary conditions, which leads to momentum quantization $k=2\pi n/L$, where $n \in Z$. A cutoff is introduced on the number of momentum eigenstates so that $n \in [-N_{\max}, N_{\max}]$, where $N_{\max}$ is a positive integer with the total number of states $N_{tot}=2N_{\max}+1$. The largest value of $N_{\max}$ which we used in the calculations in order to check the convergence was ~ 1000 although in most cases $N_{\max} \sim 500$ was sufficient. The numerical calculation can be divided into three steps.

Step I. We generate a matrix M with dimensions $2N_{tot} \times 2N_{tot}$, where the factor of 2 originates from the number of electron channels in the problem. The structure of this matrix is as follows. In the matrix element $M_{\alpha\beta}$ the indices α and β denote channel and momentum of the creation and annihilation operators in the kernel. We reserve even indices for the first channel and odd for the second channel such that the matrix element of the kernel operator between states k and k' is represented by 2×2 block in the matrix M. The difference $q=k-k'$ gives the plasmon momentum q, which is substituted into Eq. (82) with the corresponding form of the plasmon phase shifts. These phase shifts are obtained from the Eq. (82) in the case of charging interactions, Eq. (93) for

exponential interactions and can be calculated numerically using Bogoliubov equations for other interaction potentials as, for example, we have done in Sec. V C for Coulomb interactions. For the zero mode i.e., $q=0$ we use Eq. (53).

We evaluate the kernel from Eq. (82) for every set of k, k' for each channel (the kernels are different if arm lengths are not equal). Each 2×2 block with given k, k' is multiplied by the 2×2 matrix $S_{1\alpha}^{a*} S_{1\beta}^{a}$ or $S_{2\alpha}^{a*} S_{2\beta}^{a}$ (according to which channel it originates from), where $\mathcal{S}^a$ is defined in the Eq. (34). The difference of the resulting matrices gives the (k,k') block in the matrix M. From this matrix we calculate $H \equiv \exp(iM)$, which we use in the next step.

Step II. Next we generate a matrix D with dimensions $N_p \times N_p$, where $N_p = N_p^1 + N_p^2$ is the total number of particles in both channels, and N_p^μ is the number in channel μ. Convergence was achieved in most of the cases for $N_p^1 \sim N_p^2 \sim 400$. In the initial state particles occupy momentum eigenstates $-\frac{2\pi}{L}N_{\max}, \ldots, \frac{2\pi}{L}(-N_{\max}+N_p^{1,2})$. To study voltage dependence of the correlators we fix number of particles in one channel such that the states $(-\frac{2\pi}{L}N_{\max}, \ldots, 0)$ are occupied and we vary the number of electrons in another channel. The matrix D is obtained by taking matrix elements of H which correspond to occupied momentum eigenstates in the initial state.

Step III. We calculate the determinant and the inverse of the matrix D. Using this and Eq. (C13) we evaluate correlators $G_{kk'}$ in momentum space for every pair of momentum indices. Correlators in real space are obtained by performing a discrete Fourier transform of $G_{kk'}$.

[1] Y. Ji, Y. C. Chung, D. Sprinzak, M. Heiblum, D. Mahalu, and H. Shtrikman, Nature (London) **422**, 415 (2003).

[2] I. Neder, M. Heiblum, Y. Levinson, D. Mahalu, and V. Umansky, Phys. Rev. Lett. **96**, 016804 (2006).

[3] P. Roulleau, F. Portier, D. C. Glattli, P. Roche, A. Cavanna, G. Faini, U. Gennser, and D. Mailly, Phys. Rev. B **76**, 161309(R) (2007).

[4] L. V. Litvin, H.-P. Tranitz, W. Wegscheider, and C. Strunk, Phys. Rev. B **75**, 033315 (2007).

[5] I. Neder, M. Heiblum, D. Mahalu, and V. Umansky, Phys. Rev. Lett. **98**, 036803 (2007).

[6] I. Neder, F. Marquardt, M. Heiblum, D. Mahalu, and V. Umansky, Nat. Phys. **3**, 534 (2007).

[7] L. V. Litvin, A. Helzel, H.-P. Tranitz, W. Wegscheider, and C. Strunk, Phys. Rev. B **78**, 075303 (2008).

[8] P. Roulleau, F. Portier, D. C. Glattli, P. Roche, A. Cavanna, G. Faini, U. Gennser, and D. Mailly, Phys. Rev. Lett. **100**, 126802 (2008).

[9] E. Bieri, M. Weiss, O. Göktas, M. Hauser, C. Schönenberger, and S. Oberholzer, Phys. Rev. B **79**, 245324 (2009).

[10] P. Roulleau, F. Portier, P. Roche, A. Cavanna, G. Faini, U. Gennser, and D. Mailly, Phys. Rev. Lett. **102**, 236802 (2009).

[11] X. G. Wen, Phys. Rev. Lett. **64**, 2206 (1990); Phys. Rev. B **43**, 11025 (1991).

[12] C. de C. Chamon, D. E. Freed, S. A. Kivelson, S. L. Sondhi, and X. G. Wen, Phys. Rev. B **55**, 2331 (1997).

[13] F. E. Camino, W. Zhou, and V. J. Goldman, Phys. Rev. B **72**, 075342 (2005); Phys. Rev. Lett. **95**, 246802 (2005).

[14] T. Jonckheere, P. Devillard, A. Crepieux, and T. Martin, Phys. Rev. B **72**, 201305(R) (2005).

[15] K. T. Law, D. E. Feldman, and Y. Gefen, Phys. Rev. B **74**, 045319 (2006).

[16] E. A. Kim, M. J. Lawler, S. Vishveshwara, and E. Fradkin, Phys. Rev. B **74**, 155324 (2006).

[17] D. E. Feldman and A. Kitaev, Phys. Rev. Lett. **97**, 186803 (2006).

[18] V. V. Ponomarenko and D. V. Averin, Phys. Rev. Lett. **99**, 066803 (2007); Phys. Rev. B **79**, 045303 (2009); Z. Papic, N. Regnault, and S. Das Sarma, Phys. Rev. B **80**, 201303(R) (2009).

[19] D. E. Feldman, Y. Gefen, A. Kitaev, K. T. Law, and A. Stern, Phys. Rev. B **76**, 085333 (2007).

[20] I. P. Levkivskyi, A. Boyarsky, J. Fröhlich, and E. V. Sukhorukov, Phys. Rev. B **80**, 045319 (2009).

[21] D. Goldhaber-Gordon, H. Shtrikman, D. Mahalu, D. Abush-Magder, U. Meirav, and M. A. Kastner, Nature (London) **391**, 156 (1998).

[22] M. Greiner, O. Mandel, T. Esslinger, T. W. Hänsch, and I. Bloch, Nature (London) **415**, 39 (2002).

[23] G. Seelig and M. Büttiker, Phys. Rev. B **64**, 245313 (2001).

[24] F. Marquardt and C. Bruder, Phys. Rev. Lett. **92**, 056805 (2004); Phys. Rev. B **70**, 125305 (2004).

[25] H. Förster, S. Pilgram, and M. Büttiker, Phys. Rev. B **72**, 075301 (2005).

[26] V. S.-W. Chung, P. Samuelsson, and M. B. Büttiker, Phys. Rev. B **72**, 125320 (2005).

[27] F. Marquardt, Europhys. Lett. **72**, 788 (2005); Phys. Rev. B **74**, 125319 (2006).

[28] J. T. Chalker, Y. Gefen, and M. Y. Veillette, Phys. Rev. B **76**, 085320 (2007).

[29] E. V. Sukhorukov and V. V. Cheianov, Phys. Rev. Lett. **99**, 156801 (2007).

[30] I. P. Levkivskyi and E. V. Sukhorukov, Phys. Rev. B **78**, 045322 (2008).

[31] I. Neder and F. Marquardt, New J. Phys. **9**, 112 (2007).

[32] I. Neder and E. Ginossar, Phys. Rev. Lett. **100**, 196806 (2008).

[33] S.-C. Youn, H.-W. Lee, and H.-S. Sim, Phys. Rev. Lett. **100**, 196807 (2008).

[34] D. L. Kovrizhin and J. T. Chalker, Phys. Rev. B **80**, 161306(R) (2009).

[35] See: J. von Delft and H. Schoeller, Ann. Phys. **7**, 225 (1998); T. Giamarchi, *Quantum Physics in One Dimension* (Oxford University Press, Oxford, 2004).

[36] Y. Oreg and A. M. Finkelstein, Phys. Rev. Lett. **74**, 3668 (1995).

[37] J. M. Luttinger, J. Math. Phys. **4**, 1154 (1963).

[38] D. C. Mattis and E. H. Lieb, J. Math. Phys. **6**, 304 (1965).